Cycles-L: A coupled, 3-D, land surface, hydrologic, and agroecosystem landscape model

Yuning Shi[1], Felipe Montes[1], and Armen R. Kemanian[1]

[1]Department of Plant Science, The Pennsylvania State University

Key Points:

- Cycles-L is a coupled agroecosystem hydrologic modeling system that couples an agroecosystem model with a 3-D land surface hydrologic model
- Cycles-L simulated well stream discharge, grain crops yield, and nitrogen exports in the stream at a 730-ha agricultural experimental watershed
- Cycles-L can simulate landscape level processes affected by topography, soil heterogeneity, and management practices

Corresponding author: Armen R. Kemanian, `kxa15@psu.edu`

Abstract

Managing landscapes to increase agricultural productivity and environmental stewardship requires spatially distributed models that can integrate data and operate at spatial and temporal scales that are intervention-relevant. This paper presents Cycles-L, a landscape-scale, coupled agroecosystem hydrologic modeling system. Cycles-L couples a 3-D land surface hydrologic model, Flux-PIHM, with a 1-D agroecosystem model, Cycles. Cycles-L takes the landscape and hydrology structure from Flux-PIHM and most agroecosystem processes from Cycles. Consequently, Cycles-L can simulate landscape level processes affected by topography, soil heterogeneity, and management practices, owing to its physically-based hydrologic component and ability to simulate horizontal and vertical transport of mineral nitrogen (N) with water. The model was tested at a 730-ha agricultural experimental watershed within the Mahantango Creek watershed in Pennsylvania. Cycles-L simulated well stream water discharge and N exports (Nash-Sutcliffe coefficient 0.55 and 0.58, respectively), and grain crop yield (root mean square error 1.01 Mg ha^{-1}), despite some uncertainty in the accuracy of survey-based input data. Cycles-L outputs are as good if not better than those obtained with the uncoupled Flux-PIHM (water discharge) and Cycles (crop yield) models. Model predicted spatial patterns of N fluxes clearly show the combined control of crop management and topography. Cycles-L spatial and temporal resolution fills a gap in the availability of analytical models at an operational scale relevant to evaluate costly strategic and tactical interventions *in silico*, and can become a core component of tools for applications in precision agriculture, precision conservation, and artificial intelligence-based decision support systems.

1 Introduction

Managing landscapes to increase agricultural productivity and environmental stewardship requires understanding and representing landscape attributes with ever increasing fidelity. The ability to represent *in silico* the spatial variability and temporal dynamics of water and nutrient flows in such landscapes through modeling tools can help significantly in the design of cost-effective interventions in the realms of precision agriculture, precision conservation, or watershed management (Beaujouan et al., 2001; Booker et al., 2014; Stöckle et al., 2014). These modeling tools are known as spatially distributed. Two features are critical for these models to be applicable. First, they must integrate the wealth of real-time data incoming from *in situ* sensors, proximal sensing from unmanned aerial vehicles (UAVs) and terrestrial vehicles (UTVs), remote sensing from satellites, and constantly refined terrain and surface data (e.g., the Soil Survey Geographic Database or SSURGO, and the National Land Cover Database or NLCD), and meteorological data such as the Global Land Data Assimilation System (GLDAS; Rodell et al., 2004) and Europe's World Climate Research Program Coordinated Regional Downscaling Experiment (EURO-CORDEX; Jacob et al., 2014). Second, these models must operate at a scale of relevance to represent interventions and with minimal supervision, so that they do not become "mathematical marionettes" (Kirchner, 2006). There are to our knowledge only partial efforts at integrating models and data in this fashion. This paper presents the model Cycles-L, where L stands for landscape. Cycles-L integrates Flux-PIHM (Shi et al., 2013), a 3-D energy and hydrology model, and the Cycles agroecosystem model (Kemanian et al., 2022).

One-dimensional cropping system models are established tools for planning and decision making in agriculture systems with low spatial variability and high quality input data (e.g., Boote et al., 2010; Stöckle & Kemanian, 2020; Zhai et al., 2020). Applications of these 1-D models in precision agriculture lag behind their promise (Stafford, 2000) because, among other limitations (Zhai et al., 2020), the representation of both static and dynamic properties that vary spatially is limited. Although these models are often used in a gridded way in an attempt to represent spatial heterogeneity (e.g., Saarikko, 2000; Batchelor et al., 2002; Basso et al., 2007), their 1-D nature and lack of lateral water and nutrient transport among grids significantly limits their ability to represent nonlinearities in water and nutrient availability caused by topography and soil heterogeneity. An additional impedance is that using these models in a way that enriches decision-making requires substantial competence (Confalonieri et al., 2016).

There have been, however, efforts at developing models that represent spatial and temporal variability in a semi-distributed fashion in non-agricultural (Tague & Band, 2004) and agricultural landscapes without resorting to costly numerical solutions of water flow in landscapes. For example, the Soil Water Assessment Tool (SWAT; Arnold et al., 1998) and the Agricultural Policy EXtender (APEX; Gassman et al., 2010) divide the model domain into subareas (e.g., Hydrological Response Units, or HRUs) by terrain or soil attributes. Within HRUs, processes are simulated using the core of the 1-D EPIC model (J. R. Williams, 1990). In the SWAT model, HRUs do not interact; an HRU's water, nutrient, and sediment runoff contributions to the corresponding watershed outlet are represented through HRU-specific delivery ratios. However, sediment generation and delivery, for example, are not equally scaled to the HRU area, which causes output variations solely dependent on the HRU generation scheme (E. Chen & Mackay, 2004). In the APEX model, the HRUs (or subareas) are hydrologically connected, but the landscape segmentation methodology is *ad hoc* (Kemanian et al., 2009), calibration requirements are substantial (X. Wang et al., 2011), and the calibration parameters are not necessarily robust (Francesconi et al., 2014; Van Liew et al., 2017). These challenges are not unique to these modeling systems but are easily overlooked and difficult to grasp without substantial training, as alluded to in general by Confalonieri et al. (2016). Furthermore, models that aggregate large spatial scales can represent some processes very well (Arnold et al., 1998; Koch et al., 2016), but cannot represent highly non-linear processes controlled by within-subarea heterogeneity in topography, soil, and landcover. Both Stöckle and Kemanian (2020) and Tenreiro et al. (2020) concluded that among the most promising areas for improvement of current cropping system models is the representation of landscape processes that affect surface inflow and subsurface lateral flows of water and other constituents. Although efforts in this direction have been underway for decades (e.g. Beaujouan et al., 2001), the usage of spatially-distributed models remains limited. A robust, scale-independent formulation of routing is desirable to dispel uncertainty and to reduce dependence on local calibration.

Advances in computational power and modeling techniques have paved the way to the development of coupled agroecosystem hydrologic models. The Precision Agricultural-Landscape Modeling System (PALMS; Molling et al., 2005) combines an enhanced 2-D diffusive wave runoff model with a 1-D biophysical model based on the Integrated BIosphere Simulator (IBIS; Foley et al., 1996; Kucharik et al., 2000). PALMS has been used to simulate crop and erosion processes (e.g., Molling et al., 2005; Bonilla et al., 2007, 2008), and connected to other crop models (Booker et al., 2014, 2015). Although the PALMS grids are hydrologically connected at the surface, horizontal distribution of subsurface water is empiric and subsurface lateral flow is not explicitly simulated. Ward et al. (2018) presented a spatially distributed and 3-D hydrologic cropping system model, CropSyst-Microbasin (CS-MB), which added the Soil Moisture Routing model-based subsurface lateral flow to CropSyst. The model was tested in a 10.9-ha watershed growing rainfed wheat in the Inland Pacific Northwest, USA, showing promising potential to simulate field-scale spatial variability of water distribution and grain yield. The kinematic assumption used by this model, i.e., the hydraulic gradient for subsurface water flow follows the land slope rather than the water table slope, limits its application on gentle slopes (Wigmosta & Lettenmaier, 1999).

While crop production is a primary target in landscape management, more comprehensive models are needed to track dynamic processes that reshape the landscape such as soil and sediments erosion and deposition (Pineux et al., 2017) and changes in soil organic carbon stocks (Baker et al., 2007), as well as to represent the provision of ecosystem services determined by landscape diversity (Frank et al., 2012). Processes need to be represented along the continuum of soil, groundwater, and streams. For example, nitrogen (N) is both a critical plant macronutrient needed to reach high crop yield and a source of pollution (McLellan et al., 2018). Within the Chesapeake Bay Watershed (CBW), Ator and Garcia (2016) estimated that of the total N input to the CBW as fertilizer, biological N fixation, and N deposition, up to 18% is delivered to tidal waters or stored in the stream, 19% is harvested, and 45% is lost as denitrification. Most N losses occur when there is a large mismatch between N extraction in harvest and N applied as fertilizer (Woodbury et al., 2018; McLellan et al., 2018). Furthermore, high N losses as denitrification point to potentially high and unreported losses of N_2O if denitrification is incomplete (Saha et al., 2021). Opportunities exist therefore to reduce N losses in a cost-effective and environmentally friendly fashion, and taking advantage of these opportunities can greatly benefit from robust modeling and diagnostic tools.

The objectives of this paper are to present Cycles-L, a coupled agroecosystem hydrologic modeling system, and to demonstrate its use through a case study. We tested Cycles-L at an agricultural experimental watershed, WE-38, that is nested in the larger watershed of the Mahantango Creek in Pennsylvania. The long-term records of discharge and water quality, together with the surveys of crop rotations, make WE-38 an ideal site for testing Cycles-L. We evaluate and discuss the simulated discharge, stream NO_3^--N concentrations, and crop yield with observations and county-level surveys, to showcase the degree of fidelity and utility of Cycles-L for landscape level analysis.

2 Cycles-L Components Description

2.1 Flux-PIHM

Flux-PIHM is a spatially distributed land surface hydrologic model that integrates the Penn State Integrated Hydrologic Model (PIHM; Qu & Duffy, 2007; Bhatt et al., 2014) and the Noah land surface model component (F. Chen & Dudhia, 2001; Ek et al., 2003). Flux-PIHM simulates 3-D soil, groundwater, and river hydrology, along with the surface energy balance with high spatial resolution, representing land surface and hydrological variability resulting from soil, landcover, and topographic heterogeneity (Shi et al., 2015). Flux-PIHM is the core of other terrestrial biogeochemistry (Shi et al., 2018; Zhi et al., 2022) and reactive transport models (Bao et al., 2017).

In Flux-PIHM, the land surface is decomposed into unstructured triangular grids for optimal representation of local heterogeneities (topography, soil, and land cover), river channels, and watershed boundaries. River channels are represented by rectangular elements (Tarboton et al., 1991). Water transport between soil, ground, and river follows PIHM (Qu & Duffy, 2007). PIHM uses de Saint-Venant (1871) equations to compute channel (1-D) and surface (2-D) water flow. Infiltration at the air-soil interface is calculated using the properties of the top 10 cm of soil following Darcy's law. In the subsurface, the prismatic and triangular volume is divided into water saturated and unsaturated zones. Unsaturated water transport only occurs vertically. In the saturated zone, groundwater flow is horizontal with dynamic coupling to the unsaturated zone across the water table, governed by Darcy's law. The hydrologic equations at each model grid are discretized to ordinary differential equations (ODEs), which are assembled within the boundaries of the domain, and solved simultaneously using the CVODE ODE solver (Hindmarsh et al., 2005). The land surface component of Flux-PIHM is adapted from the Noah land surface model (F. Chen & Dudhia, 2001; Ek et al., 2003), and is coupled to PIHM by exchanging water table depth, infiltration rate, water table position, net precipitation rate, and evapotranspiration rate between the two components. The land surface component simulates surface energy balance, snow melt, interception, and drip. In the land surface component, the subsurface is divided into layers with fixed thickness. By default, the soil layer thickness increases from 0.11 m for the first layer to 0.38 m for the 10th layer (Shi et al., 2015). The number of soil layers can be reduced, and the thickness of the deepest layer can be adjusted to match the depth to bedrock. If the bedrock is deeper than the total thickness of 10 soil layers, one additional layer is added as needed. While PIHM only simulates infiltration rate, lateral subsurface flow rate, and position of water table for all model grids, these variables are used as boundary conditions by the land surface model to calculate transport within the unsaturated zone using the Richards equation. A recent development is adding a topographic solar radiation module to Flux-PIHM (Shi et al., 2018). Flux-PIHM is now the core landscape hydrology model for multiple modeling systems. Detailed descriptions of PIHM and Flux-PIHM are provided by Qu and Duffy (2007), and Shi et al. (2013, 2014, 2018).

2.2 Cycles

Cycles is a one-dimensional process-based multi-year and multi-species agroecosystem model (Kemanian et al., 2022). Cycles evolved from C-Farm (Kemanian & Stöckle, 2010) and shares biophysical modules with CropSyst (Stöckle et al., 2014). Cycles simulates the water and energy balance, the coupled cycling of carbon (C) and N, and plant growth at daily time steps. Evapotranspiration is calculated based on the Penman-Monteith equation. Transpiration is modulated by temperature, crop root distribution, soil water potential, and plant hydraulic properties (Campbell, 1985). Plant development is determined by thermal time, and plant growth is based on solar radiation interception (light limited) or the realized transpiration (water limited) based on stomatal optimization theory (Cowan, 1978, 1982; Katul et al., 2009). Soil organic C and N cycling are based on saturation theory (Kemanian & Stöckle, 2010; Pravia et al., 2019). The model can simulate a wide range of perturbations of biogeochemical processes caused by management practices such as tillage, irrigation, organic and inorganic nutrient additions, annual and perennial crop selections, crop harvests as grain or forages, polycultures, relay cropping, and grazing. Cycles can simulate unlimited plant species as specified by the user.

2.3 Cycles-L

Cycles-L (Fig. 1) takes the landscape and hydrology structure from Flux-PIHM and most agroecosystem processes from Cycles. The surface energy balance and soil hydrology are simulated as in Flux-PIHM, except for plant water uptake, hydraulic lifting, and the water balance of surface plant residues, which use Cycles' algorithms. Hydrologic processes are simulated with a sub-daily time step (usually $\sim 10^0$ minute, dynamic). Following Cycles, each soil layer has texture- and organic matter-dependent hydraulic properties. However, when activating landscape hydrology, the properties of the soil profile are averaged preserving total soil mass and porosity to allow solving for vertical and lateral fluxes using Flux-PIHM. Biogeochemical processes are simulated with a daily time step independently for each soil layer. Tillage operations allow mixing all components of the soil layers affected by tillage. The one-dimensional Cycles model is integrated into every Flux-PIHM model grid, therefore each model grid can be assigned with a unique land cover or crop rotation.

A solute transport module is used to simulate subsurface nutrient transport. This model is the same as the subsurface transport in Flux-PIHM-BGC (Shi et al., 2018), and is used to calculate total solute flowing in or out of a model grid:

$$V_i \frac{\mathrm{d}}{\mathrm{d}t}\left(\Theta_i C_i\right) = \sum_j \left(-q_{ij} C_{ij}\right) + F, \tag{1}$$

where V_i is the subsurface prism volume of grid i (m^3), C_i is the subsurface mineral N concentration (kg m^{-3}), Θ_i is the volumetric soil water content (m^3 m^{-3}), q_{ij} is the lateral water flow at the subsurface between grid i and its neighbor at edge j (m^3 s^{-1}), and F is a source/sink term of the corresponding solute (kg s^{-1}). In Cycles-L, the source/sink

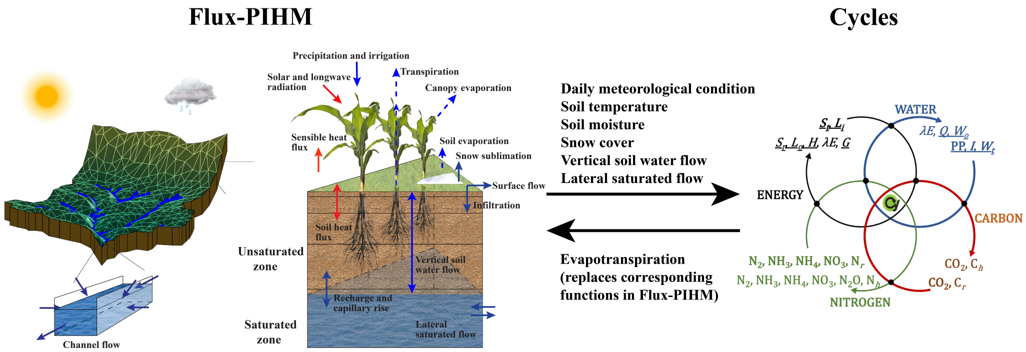

Figure 1. Schematic illustration of land surface and hydrologic processes simulated by Flux-PIHM; energy, water, carbon (C) and nitrogen (N) cycles simulated by Cycles with fluxes in and out for each component; and the coupling between Flux-PIHM and Cycles. For Cycles, the nodes at the arrows' intersections represent interactions between cycles; S_t and L_i are incoming shortwave and longwave radiation, S_r and L_o are outgoing shortwave and longwave radiation, H, λE, and G are sensible, latent, and ground heat fluxes, PP is precipitation, I is irrigation, W_t is capillary rise, Q is runoff, W_o is soil percolation or lateral flow, C_r and N_r are C and N changes caused by soil amendments, and C_h and N_h are harvested C and N. When coupled, the processes represented by dashed arrows in Flux-PIHM are simulated by Cycles, and the fluxes with underlines in Cycles are calculated by Flux-PIHM.

terms for mineral N are:

$$\begin{aligned}\frac{\mathrm{d}}{\mathrm{d}t}\mathrm{NO_3^-\text{-}N} = {} & \mathrm{NO_3^-\text{-}N}_f + \mathrm{NO_3^-\text{-}N}_d + \mathrm{NO_3^-\text{-}N_{nit}} + \mathrm{NO_3^-\text{-}N_{imm}} \\ & - \mathrm{NO_3^-\text{-}N_{dnit}} - \mathrm{NO_3^-\text{-}N_{pup}} - \mathrm{NO_3^-\text{-}N}_l - \mathrm{NO_3^-\text{-}N}_r\end{aligned} \tag{2a}$$

and

$$\begin{aligned}\frac{\mathrm{d}}{\mathrm{d}t}\mathrm{NH_4^+\text{-}N} = {} & \mathrm{NH_4^+\text{-}N}_f + \mathrm{NH_4^+\text{-}N}_d + \mathrm{NH_4^+\text{-}N_{min}} \\ & - \mathrm{NH_4^+\text{-}N_{nit}} - \mathrm{NH_4^+\text{-}N_{imm}} - \mathrm{NH_4^+\text{-}N_{pup}} - \mathrm{NH_3\text{-}N_{vol}} - \mathrm{NH_4^+\text{-}N}_l - \mathrm{NH_4^+\text{-}N}_r\end{aligned} \tag{2b}$$

where subscript f is for fertilizer, d for deposition, nit for nitrification, imm for microbial immobilization or microbial uptake, pup for plant uptake, dnit for denitrification, l for leaching or percolation, r for runoff, min for mineralization of organic compounds with N (many), and vol for volatilization as $\mathrm{NH_3}$-N. Note that $\mathrm{NO_3^-\text{-}N_{nit}}$ and $\mathrm{NH_4^+\text{-}N_{nit}}$ are the same, and $\mathrm{NH_4^+}$ and $\mathrm{NO_3^-}$ are just N species identifiers. If the net water flow from a grid is outward (net efflux from grid i to grid j) then the mineral N concentration (C_{ij}) of the water flow (q_{ij}) is that of grid i: $C_{ij} = C_i$; otherwise, $C_{ij} = C_j$. In Flux-PIHM, horizontal water flow is restricted to the saturated zone. But this horizontal flow is calibrated to include the representation of lateral perched flow above unsaturated layers and that flow can drag mineral N (M. R. Williams et al., 2015) or other solutes. This is difficult to predict because it depends on the mixing between water flowing through macropores and water in the non-macropore soil matrix and the distribution of mineral N. To account empirically for that transport, we tentatively assigned a weight function that allows for mineral N transport from unsaturated layers. The weighting function is $\frac{K_r}{D-d_z}$, where K_r is the relative hydraulic conductivity (hydraulic conductivity divided by saturated hydraulic conductivity), D is the total soil depth, and d_z is the depth of the corresponding soil layer. This function is applied to all soil layers when calculating the average concentration of soil mineral N, to emulate the horizontal transport of mineral N in the shallower depths with higher hydraulic conductivities. Due to the very low hydraulic conductivity of dry layers, they contribute little to mineral N transport.

At the beginning of each simulation day, land surface processes are calculated first using the Noah land surface model. Note that in Cycles-L, Noah LSM evapotranspiration functions are replaced by the corresponding Cycles functions. Cycles then applies management operations and simulates vegetation, residue, and soil C and N processes, using as input the daily meteorological conditions, soil temperature, soil moisture, and snow cover informed by Flux-PIHM. Cycles passes evapotranspiration rate and N fluxes as source/sink terms in water and N transport. Then, Flux-PIHM calculates the transport of water and N for the entire domain using sub-daily time steps.

3 Site and data

3.1 Description of the WE-38 watershed

The WE-38 watershed is a 7.3 km^2 first-order watershed within the Mahantango Creek Watershed in Pennsylvania's Northumberland county (Fig. 2a). Elevation ranges from 503 m at the northernmost ridge to about 214 m near the southern outlet. The land cover comprises cultivated land (55%), followed by forests (40%), pasture (3%), and developed area (2%). The watershed contains more than 300 farm fields. Surveys and interviews were used to obtain field-specific operations (Veith et al., 2015) that documented crop species, planting and harvesting dates, tillage tools and operation dates, and synthetic fertilizer and animal manure application rates and dates. The watershed has been the focus of rigorous research on agricultural management and monitoring of water quality (Pionke et al., 2000; Bryant et al., 2011; Buda et al., 2011; Church et al., 2011; Lu et al., 2015; Veith et al., 2015), and long-term discharge and water quality measurements, including NO_3^--N and NH_4^+-N, are publicly available.

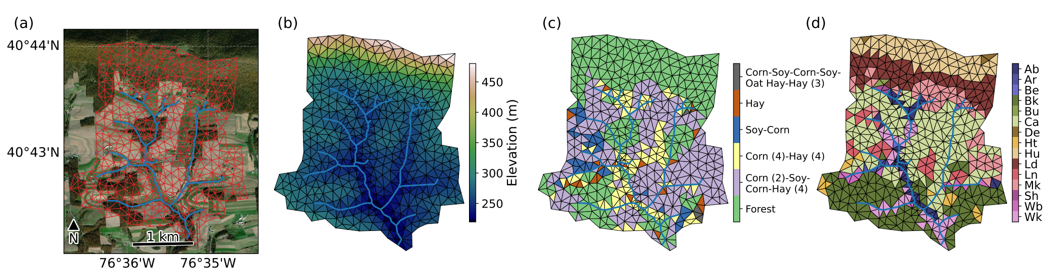

Figure 2. (a) WE-38 model domain projected onto an aerial photograph of the watershed. The red triangles represent the model grids and the blue lines represent river segments. (b) Surface elevation map of the WE-38 model domain. (c) Land use and crop rotations in the WE-38 model grids. (d) SSURGO soil map projected onto WE-38 model grids, with each color representing one unique soil type. The soil series are Albrights silt loam (Ab), Alvira silt loam (Ar), Bedington silt loam (Be), Berks channery silt loam (Bk), Buchanan channery loam (Bu), Calvin-Klinesville shaly silt loams (Ca), Dekalb very channery sandy loam (De), Hartleton channery silt loam (Ht), Hazleton and Clymer extremely stony sandy loams (Hu), Laidig and Meckesville extremely stony soils (Ld), Leck kill shaly silt loam (Ln), Meckesville silt loam (Mk), Shelmadine silt loam (Sh), Watson silt loam (Wb), and Weikert and Klinesville shaly silt loams (Wk).

3.2 Domain and model setup

The Cycles-L WE-38 model physical domain consists of 114 segments representing the stream network (average 98-m long) and 883 triangular grids (average 0.83 ha), of which 522 triangular grids are cropland (Fig. 2). The watershed drainage network was mapped using the Terrain Analysis Using Digital Elevation Models tool (TauDEM; Tarboton et al., 2009; Tarboton, 2015) on a digital elevation model (DEM) obtained from light detection and ranging (lidar) data and color orthophotography at horizontal and vertical resolutions of 0.5 and 0.15 m, respectively (Bryant et al., 2011). Afterwards, the drainage network was updated by overlapping the TauDEM analysis results with a georeferenced orthomosaic of the watershed obtained from the Pennsylvania Spatial Data Access (PASDA, 2022).

To represent field operations, we converted the database used for WE-38 in Hirt et al. (2020) to Cycles-L inputs. This database aggregates field operations history by crop in the rotation. These rotations and associated field operations were projected on the Cycles-L WE-38 model domain (Fig. 2c). Model grids were assigned to one of six land uses: deciduous forest, a corn (2 years)-soybean-corn-hay (4 years) rotation, a corn (4 years)-hay (4 years) rotation, a soybean-corn rotation, a hay rotation, and a corn-soybean-corn-soybean-oat hay-hay (3 years) rotation. Hay was simulated as a mixture of 1/3 alfalfa and 2/3 orchardgrass. Deciduous forest is the most common land use type, while the corn (2 years)-soybean-corn-hay (4 years) rotation is the most common crop rotation. The operations for each crop are listed in Table 1.

To prevent an unrealistic rotation synchrony in grids with the same rotation, we randomly assigned a different starting point in the rotation to each grid within the assigned rotation. For example, for the model grids with the soybean-corn rotation, we randomly assigned half of those grids to start with soybean, and the other half to start with corn.

The soil properties texture, organic matter, and bulk density (by layer) were extracted from the SSURGO database projected to the model domain (Fig. 2d); 15 unique soil series were identified for the watershed. The meteorological forcing (precipitation, air temperature, humidity, wind speed, downward solar radiation, downward longwave radiation, and air pressure) were obtained from the North American Land Data Assimilation System Phase 2 (NLDAS-2; Xia et al., 2012) forcing data, which provides data at hourly time-step and is suitable for hydrologic simulations.

For model testing, annual crop yields were downloaded from the The United States Department of Agriculture (USDA) National Agricultural Statistics Service (NASS) at county level (Northumberland county) and compared with both Cycles 1-D and Cycles-L for the entire watershed.

The simulation period was 16 years from 0000 UTC 1 January 2000 to 0000 UTC 1 January 2016. Setting up the model requires spin-up to stabilize hydrological and biogeochemical soil properties. The spin-up process was divided into two, one for hydrology and one for soil variables. Because running Cycles-L is more computationally expensive than Flux-PIHM, we first ran Flux-PIHM for land surface hydrological parameter calibration and hydrological state spin-up. When running Flux-PIHM, the forest was simulated as the deciduous forest NLCD land cover type, the hay rotation was simulated as the pasture/hay land cover type, and all other crop rotations were simulated as the cultivated crop land cover type. The leaf area index (LAI) forcing was prescribed monthly climatological LAI that depends on land cover types. Flux-PIHM hydrologic and land surface parameters were manually calibrated using the observed discharge data from 2000 to 2011. Model parameters that affect horizontal flow and key parameters identified from Flux-PIHM sensitivity analyses (Shi et al., 2014; Xiao et al., 2019) were adjusted, including vertical and horizontal saturated hydraulic conductivities, vertical and

Table 1. Field operations for crops in the rotation. The N-P-K refers to the proportion of N, P, and K in the dry mass. For manure, 25% of N is added as NH_4^+ and 75% as organic N with C:N ratio of 14. For hay, fertilization follows after a clipping and haying event.

Opearation	Day of year	Fertilizer mass (kg ha^{-1})	Fertilizer N-P-K
	Corn		
Manure fertilizer	100	3500	03-01-00
Tillage moldboard	101		
Tillage disking	102		
Planting	121		
Fertilization	121	100	10-20-20
Fertilization	152	100	33-00-00
Harvest and kill crop			
	Soybean		
Manure fertilizer	100	1875	03-01-00
Tillage disking	102		
Planting	121		
Harvest and kill			
	Oat for hay		
Tillage chisel + cultivator	92		
Planting	97		
Fertilization	97	300	03-15-48
Fertilization	166	100	33-00-00
Harvest and kill	219		
	Hay (alfalfa + orchardgrass for hay)		
Tillage (year 1)	101		
Planting (year 1)	105		
Fertilization manure (year 1)	100	3500	03-01-00
Fertilization (year 1)	259	100	02-11-45
Clipping and haying (4 times)	Various		
Fertilization all years (4 times)	Various	100	02-11-45
Kill (year 4)	303		

horizontal saturated macropore hydraulic conductivities, macropore depth, soil porosity, van Genuchten parameters, and canopy stomatal conductance. After calibration, land surface and hydrological states were spun up by recycling the meteorological forcing. Hydrological states are considered steady when the change of watershed average groundwater storage is lower than 1 cm between the beginning and end of a simulation cycle. Steady state condition was reached in 32 years, which required recycling the meteorological forcing twice.

The land surface hydrological state variables after the spin-up were used to initialize the Cycles-L spin-up process. The Cycles-L model was run repeatedly by recycling the 16-year meteorological forcing and prescribed farm operations until the change of soil profile organic carbon was lower than 0.01 Mg ha^{-1}. Cycles-L reached steady state conditions after 11 simulation cycles, i.e., 167 simulation years.

We calibrated the crop model using the USDA-NASS survey corn yield by adjusting crop ecophysiological parameters that are site-dependent (rooting depth) and two related parameters that regulate growth potential, the radiation use efficiency (g of biomass accrued per MJ of radiation intercepted) and transpiration use efficiency (g of biomass accrued per kg of water transpired). The last two parameters were reduced to 2/3 of their default values, to represent in a simplified way limitations to growth not accounted for in the input data (shallower soils or compacted layers) or in the model (deficient root exploration due to rocks); the watershed soils can have locally high rock content (Saha et al., 2017). Overestimating yields can severely alter outputs mostly by increasing nutrient extraction in harvested grain or forage.

Uncoupled Cycles simulations were performed to compare with Cycles-L outputs. The Cycles 1-D simulations used the most dominant soil type Calvin-Klinesville shaly silt loams (Ca), and the most prevailing crop rotation [corn (2 years)-soybean-corn-hay (4 years)]. As in Cycles-L, we ran four Cycles simulations, starting with different crops in the rotation, i.e., a corn (2 years)-soybean-corn-hay (4 years) simulation, a soybean-corn-hay (4 years)-corn (2 years) simulation, a hay (4 years)-corn (2 years)-soybean-corn simulation, and a hay (2 years)-corn (2 years)-soybean-corn-hay (2 years) simulation. Results from the four simulations were averaged to be compared with Cycles-L.

4 Results

4.1 Simulation of stream discharge

Model simulation results from 2000 to 2015 after spin-up are presented below, and evaluated using field measurements or surveys.

Cycles-L captured the interannual variability of discharge, and accurately predicted the timing of most discharge events. The base flow rate predicted by Cycles-L compared well with observations. The Nash-Sutcliffe coefficient (NSE) of daily discharge for the entire simulation period was 0.55. The NSE, however, varied from year to year, and was as high as 0.85 in 2005. Discharge from multiple years was also averaged to each day of year to glean within-year patterns of measured and modeled discharge (Fig. 3b). The model captured the seasonal wet-dry cycles, and the predicted magnitude of discharge generally agreed well with observation. Cycles-L slightly overestimated discharge, except for late winter and spring. The NSE for the predicted multi-year average discharge was 0.68.

Flux-PIHM prediction was similar to Cycles-L (Fig. 3a) because both of them share the same hydrologic component but canopy cover is endogenous in Cycles-L and a forcing in Flux-PIHM. The NSE for Flux-PIHM daily discharge prediction was 0.60, which was slightly higher than Cycles-L (0.55). It should be noted that the land surface and hydrologic parameters in Cycles-L were calibrated by running Flux-PIHM, which may

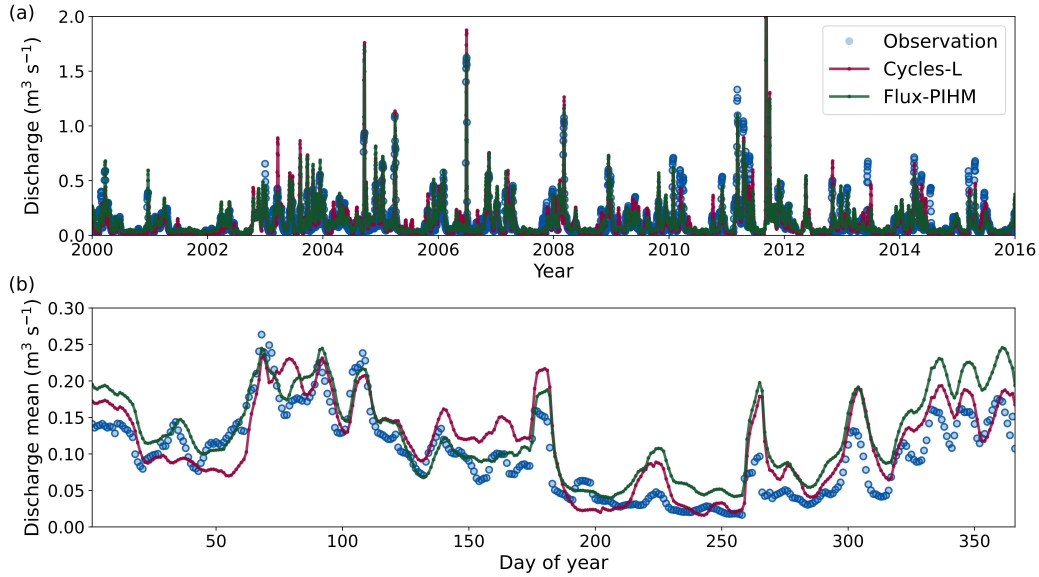

Figure 3. (a) Comparison of daily discharge between observations and outputs from Cycles-L and Flux-PIHM, from 1 Jan 2000 to 31 Dec 2015. (b) Comparison of daily discharge when averaged to each day of year.

cause Flux-PIHM to yield slightly better performance than Cycles-L. When averaged to each day of year, Flux-PIHM also tended to overestimate discharge. Compared to Cycles-L, Flux-PIHM produced higher predictions of discharge in spring, and lower predictions in other seasons.

4.2 Simulation of grain yield

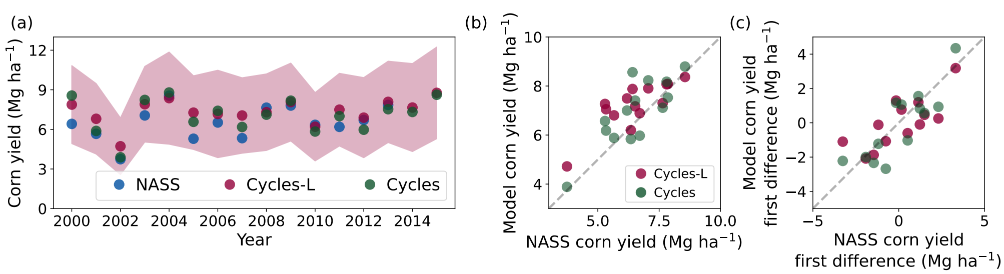

Figure 4. (a) Temporal variation of USDA-NASS survey corn yield and both Cycles-L and Cycles 1-D predicted annual average corn yield from 2000 to 2015. The USDA-NASS survey is for Northumberland County, PA. The shaded area represents the standard deviations of corn yield in space. (b) Cycles-L and Cycles 1-D predicted annual average corn yield versus USDA-NASS survey annual corn yield. (c) First difference of Cycles-L and Cycles 1-D predicted annual average corn yield versus first difference of USDA-NASS survey annual corn yield.

On average, both Cycles-L and Cycles captured the corn yield variation well (Fig. 4), with R^2 of 0.66 for Cycles-L and 0.65 for Cycles, and root mean square error (RMSE) of 1.01 and 0.90 Mg ha^{-1} for Cycles-L and Cycles, respectively. When comparing the first differences of corn yield, which detrend yield increases with time due to technology, the R^2 for Cycles-L decreased to 0.58 and that for Cycles increased to 0.72. Cycles-L tended to underestimate the interannual variability compared to Cycles (Fig. 4c). The shaded area in Fig. 4(a) illustrates the spatial variation of corn grain yield predicted by Cycles-L. The spatial variation of corn yield was larger when yield was higher, and smaller when yield was lower. The standard deviations of corn yield in space varied between 2.2 and 3.5 Mg ha^{-1}. The USDA-NASS survey reported yields were always within the predicted one-standard-deviation (Fig. 4a).

4.3 Simulation of mineral nitrogen discharge

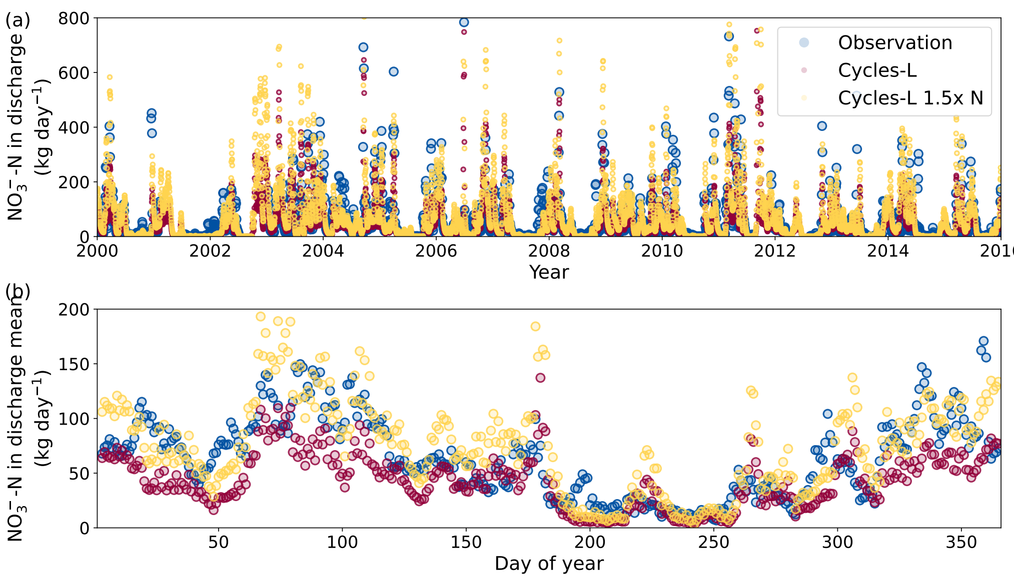

Figure 5. (a) Comparison of daily nitrate-N discharge between the observations and two Cycles-L simulations (1x N and 1.5x N), from 1 Jan 2000 to 31 Dec 2015. (b) Comparison of daily nitrate-N discharge when averaged to each day of year. When averaged to each day of year, a 3-day moving average was applied to both observations and predictions to better reveal the temporal patterns.

We focused on the N exported at the watershed outlet, where comparisons with measurements allow a reality-bounded assessment of the impact of changing N fertilization rates. The temporal patterns of water discharge (Fig. 3) and N discharge (Fig. 5) are similar, because N discharge is controlled by water discharge. Accordingly, the N discharge pattern was correctly simulated by Cycles-L with an NSE of 0.58, but the N mass discharged through the stream was consistently underestimated compared with measurements (Fig. 5). The observed and predicted average NO_3^--N discharge were 63.8 and 46.1 kg day^{-1}.

4.4 Simulation of mineral nitrogen concentration in the stream

Because the stream discharge was slightly overestimated and NO_3^--N underestimated, the concentration of NO_3^--N was also underestimated, as was the seasonal variation in NO_3^--N concentration (Fig. 6). The average observed NO_3^--N concentration in the stream was 5.4 mg L^{-1}, with a pronounced W-shaped seasonal pattern with highs in early summer and in winter, and lows in spring and autumn (Fig. 6b). Interannual variability was also noticeable. The simulations consistently underestimated the concentration of NO_3^--N,

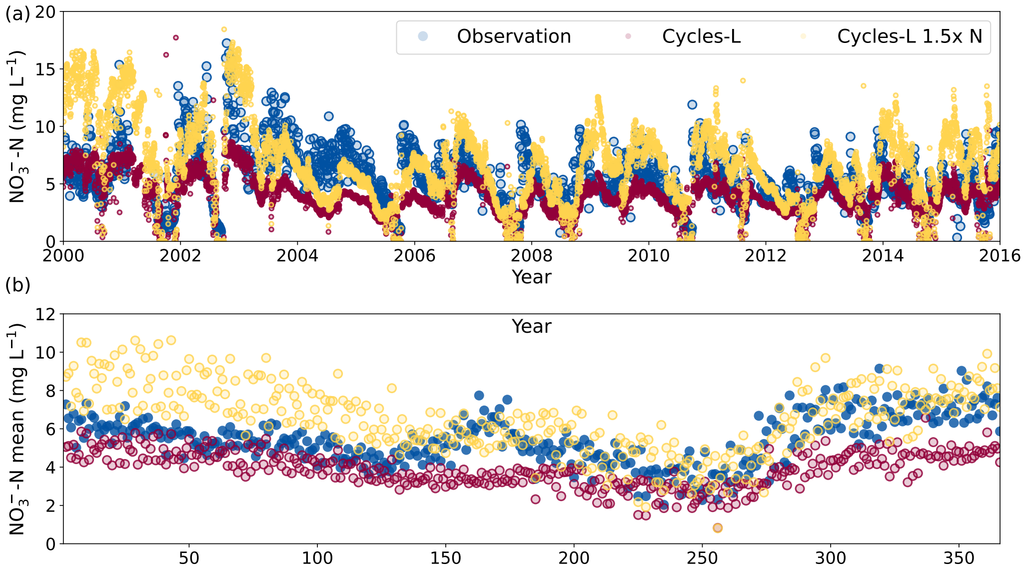

Figure 6. (a) Comparison of daily stream nitrate-N concentrations between observations and two Cycles-L simulations (1x N and 1.5x N), from 1 Jan 2000 to 31 Dec 2015. (b) Comparison of daily nitrate-N concentrations when averaged to each day of year.

on average by about 30%, and significantly underestimated the magnitude of seasonal variations.

4.5 Spatial pattern of simulated nitrogen fluxes

Table 2. Simulated and observed nitrogen fluxes. All fluxes are watershed annual average.

N flux	Cycles-L	Cycles-L 1.25xN	Cycles-L 1.5xN	Observed
		(kg ha^{-1} yr^{-1})		
Fixation and deposition	45.0	41.9	38.7	N/A
Fertilization (manure)	54.8	68.4	82.2	N/A
Fertilization (synthetic)	30.2	37.8	45.3	N/A
Volatilization	9.4	10.6	11.8	N/A
Denitrification	8.4	10.7	13.3	N/A
N_2O emission from nitrification	0.5	0.6	0.7	N/A
N in Harvest	77.3	83.7	89.1	N/A
N in discharge	22.7	29.9	38.8	31.4

Since the model has been run to steady state, the change of N storage in the system was low. On average, most N removals other than discharge occurred through N harvest, NH_3-N volatilization, and NO_3^--N denitrification (Table 2).

Due to the distribution of the cropland and forestland, N inputs had a marked spatial distribution (Fig. 7). Yet, the spatial patterns of N losses were also shaped by topography and soils that alter hydrology. The spatial pattern of N input was clearly controlled by crop management. Forests and the areas with the hay rotation have low N in-

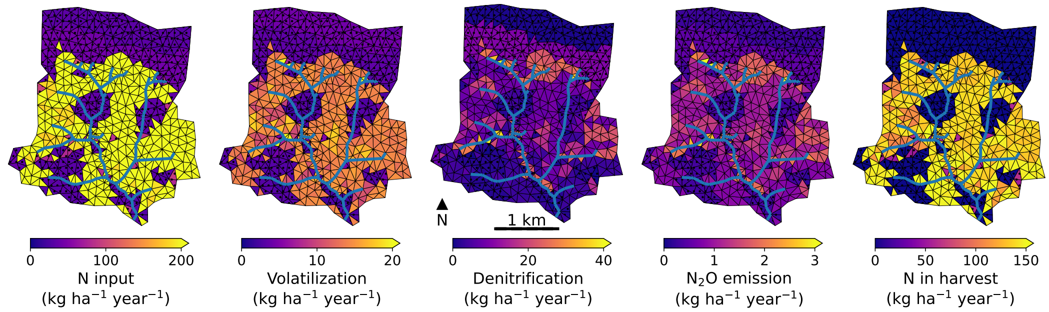

Figure 7. Spatial patterns of nitrogen fluxes (nitrogen input, nitrogen volatilization, denitrification, N_2O emission, and nitrogen in harvest) as predicted by Cycles-L. For each model grid, the fluxes were averaged over the whole simulation period. The dotted areas represent the forests and areas with the hay rotation. The blue lines represent river segments.

put because there was no fertilization but only deposition and biological fixation. The spatial pattern of NH_3-N volatilization was highly correlated with the pattern of fertilization. The spatial patterns of denitrification and N_2O emission demonstrate the complex interactions between crop management and topography. The forests had a lower denitrification rate (and N_2O emission) compared to areas with crop rotations. For the areas with crop rotations, denitrification rates (and N_2O emission) were higher in headwaters and some regions of convergent flow or flat terrain near the stream (but not all), where soil water content was higher. Nitrogen harvest was largest in areas with a high frequency of corn and soybean.

5 Discussion

5.1 Simulating hydrology

Cycles-L captured the interannual variability of discharge, and accurately predicted the timing of peak discharge events and base flow rates with minimum manual calibration. This is in line with the high fidelity of the PIHM family models demonstrated for multiple watersheds (Shi et al., 2013, 2015; Jepsen et al., 2016; Crow et al., 2018; Zhang et al., 2018; Xiao et al., 2019; Zheng et al., 2021). Among the desirable future improvements are to represent explicitly perched water movement on top of Bt horizons, which would allow lateral water transport overlaying unsaturated soil layers. Currently, this process is lumped in the lateral flow calibration parameters. While modeling it explicitly may not improve the overall accuracy of discharge predictions, it may affect mineral N (and other constituents) transport. Similar considerations apply to modeling water flux through tile drains, with the practical caveat that the location of tile drains is often unknown. When the tile drain network is well mapped it can be explicitly simulated although at the cost of a very dense grid (De Schepper et al., 2015). Nonetheless, while the model performs well in its current formulation, future developments should include an explicit representation of tile drains as submerged channels that interact with groundwater.

Compared with other spatially distributed agroecosystem hydrological systems, which usually have rigid rectangular model grids, the unstructured triangular grids of Cycles-L provides both computational efficiency and optimal representations of local heterogeneity. Unstructured triangular grids capture with ease watershed boundaries, stream networks, and soil and vegetation units (Qu & Duffy, 2007; Kumar et al., 2010; De Schepper et al., 2015). Because grid sizes can differ in Cycles-L, coarser grids can be used in locations with simple topography and low land surface heterogeneity to improve model efficiency, while finer grids can be used to capture complex topography and spatial heterogeneity in soil and vegetation, an approach that is already suggested by the unstructured mesh used to represent tile drains by De Schepper et al. (2015). These features enable applications for precision agriculture in a cohesive framework. Cycles-L's unique capability to simulate the two-way interaction between stream and riparian zones makes it extremely useful to evaluate interventions in agricultural areas along floodplains where flooding damage risk is high (Collins et al., 2022).

5.2 Simulating nitrogen discharge and concentration

When using the fertilization rate as prescribed by the survey data (Hirt et al., 2020), the model prediction of water discharge and corn yield agreed well with the observations and survey (Figures 3 and 4), but underestimated the stream NO_3^--N concentration and NO_3^--N discharge (Figures 5 and 6). The discharge underestimation amounted to 9.7 kg ha^{-1} y^{-1} of N (Table 2). Among the possible reasons are that the model is overestimating other N losses or that N inputs are underreported. Therefore, we ran exploratory Cycles-L simulations with arbitrary N input increases of 25% (not shown in the figures) and 50% over the survey data (hereafter, Cycles-L 1.25x N and Cycles-L 1.5x N simulations).

The NO_3^--N in discharge predicted by the Cycles-L 1.5x N simulation was higher than the observed discharge (+7.4 over the observed 31.4 kg NO_3^--N ha^{-1} y^{-1}) but closer to that in the default simulation; the NO_3^--N in discharge predicted with Cycles-L 1.25x N almost matched the observed discharge (Table 2). Although the 1.5x N simulation overestimated stream NO_3^--N concentration in winter and spring, deviations in multi-year average N discharge for this time period were small, because the model's underestimation of water discharge for the same time period (Fig. 3b) compensated for deviations in NO_3^--N concentration. The 1.5x N simulation substantially overestimated NO_3^--N concentration in 2000 and 2001 and underestimated it in 2003 and 2004 (Fig. 6). For other years, the predicted NO_3^--N concentration agreed well with observations, especially for the second half of the simulation (from 2008 to 2016), despite missing some peaks. When averaged to each day of year, the model captured the seasonal variation of NO_3^--N concentration change, but overestimated the concentration in late winter and early spring (Fig. 6b).

The Cycles-L 1x N, 1.25x N, and 1.5x N simulations produced almost identical corn yield and water discharge. It suggests that crop growth was not N limited in WE-38 even when using the 1x fertilization rate. Because crop growth was similar between the two simulations, evapotranspiration simulations were close as well, hydrology was not affected, and the three simulations produced similar stream discharge. Adding more N fertilizer, however, increased stream N concentration. It should be noted that adding 50% more N fertilizer did not increase N inputs to the watershed proportionally because of a parallel reduction in N biological fixation of 6.3 kg ha^{-1} y^{-1} of N (Table 2). If we were to assume that indeed, inputs of N were underestimated, and that they would scale linearly between our 1x and 1.5x simulations, we estimate that N inputs obtained through surveys were underestimated by 25 to 30%.

As in Ator and Garcia (2016), denitrification was a significant loss pathway. When spatially averaged over the whole simulation period (from 2000 to 2015), denitrification rates generally increased as N input increased within each crop rotation type (Fig. 8), but strong variation existed depending on the rotation and field location. There seems to be a correlation between well drained locations and the location of corn and soybean in the field (Fig. 2), likely reflecting producers' choices that facilitate field operations in cash crops, which may result in lesser than expected N denitrification losses in those fields (Fig. 8). However, NO_3^--N is transported mostly through groundwater, and grids that gain NO_3^--N through leaching from other grids may have higher denitrification rates than

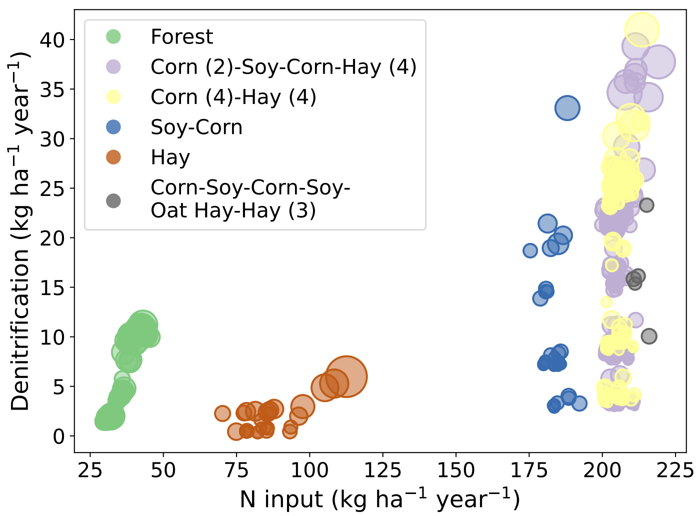

Figure 8. Average denitrification rate vs average nitrogen input as predicted by Cycles-L. Each circle represents one model grid, averaged over the whole simulation period. The sizes of the circles represent the degrees of soil saturation. Different colors represent different land uses/crop rotations.

those expected based only on surface N input. While forests and hay fields have lower N input than the other crop rotations, most cropping model grids have average N input between 175 and 225 kg ha^{-1} y^{-1}, but their simulated denitrification rates varied significantly, from around 5 to 40 kg NO_3^--N ha^{-1} y^{-1}, in large part due to hydrological control of leaching and denitrification. The movement of water alters both NO_3^--N and oxygen availability in space, which leads to significantly different spatial denitrification rates (Groffman et al., 2009). Within each crop rotation type, denitrification rates tend to increase when soil wetness increases (represented by the circles' size in Fig. 8), which reflects the dominant control of oxygen on denitrification rates in the model (i.e., air filled pore space decreases and so does oxygen replenishment). The importance of representing these spatial interactions to model hot spots and hot moments of denitrification has been highlighted earlier by Groffman et al. (2009) and measured in the field by Saha et al. (2017). Our modeling framework advances in that direction. Improvements are needed to represent denitrification in stream sediments and to include physical features such as the specific location of buried carbon sources (Hill et al., 2014), to further refine our understanding and modeling of denitrification spatial distribution (Wallace et al., 2020).

5.3 Strength of Cycles-L and opportunities for improvement

Because of its spatially distributed nature, Cycles-L represents a step forward to simulate landscape level processes such as groundwater and stream water transport of reactive N and other compounds as affected by crop rotation, soil type, and weather variations within the watershed domain. It can also represent the heterogeneity of agroecosystem processes caused by topography, soil heterogeneity, and management practices, owing to its physically-based hydrologic component and ability to simulate horizontal and vertical transport of mineral N with water. By extension, other nutrients like soluble phosphorus (McConnell et al., 2020), dissolved organic C (Pabich et al., 2001), and agrochemicals (Hladik & Kolpin, 2015) can be integrated in the same framework.

Cycles-L can be an important tool to evaluate costly interventions *in silico* before deployment in the field, as complex interactions among subsurface, land surface, and crops can be explored before committing resources on the ground, as exemplified by a comparable model using a square grid domain (Beaujouan et al., 2001). Similarly, Cycles-L can become a powerful tool for precision agriculture and precision conservation, becoming a core component of artificial intelligence applications (Gil et al., 2021). The spatial and temporal richness of the model outputs coupled with immersive visuals open new opportunities to represent the dynamics of agroecosystems to develop research, educational, and public engagement tools (C. Wang et al., 2019).

Comparing Cycles 1-D average corn yield with county-level yield averages, a coarse comparison due to the amalgamation of disparate scales, indicates that overall Cycles correctly captures the effect of interannual variations in weather on crop yield. So do other 1-D cropping system models applied in the region (Castaño-Sánchez et al., 2020). Cycles-L did not improve upon these results, although the comparison scope is limited to this small watershed. The simulations with Cycles-L increased the minimum yield most likely due to redistribution of subsurface water in drier years. It remains to be tested if an even finer resolution (smaller triangles) would render a better representation of hydrology and crop growth and yield. Such finer resolution would also require using dense, grid-specific soil input information. While such soil information might not be available, yield maps that would allow such testing are already regularly available, and assessing the effect of a finer resolution in representing certain processes is needed to advance applications in precision agriculture.

Macropore flow in Flux-PIHM lumps vertical bypass flow, but also fast lateral flow of perched water that reaches the stream with lesser mixing with water in the non-saturated soil matrix. In this watershed, measurements have revealed that water can reach streams through ephemeral springs that exfiltrate after lateral transport (Redder et al., 2021), and that water can have high concentration of NO_3^--N that reflects limited mixing with groundwater (M. R. Williams et al., 2015). When measuring in-stream NO_3^--N concentration, this spring contribution of water and NO_3^--N can cause spikier readings in stream NO_3^--N concentration than when water reaching the stream is mixed with groundwater, and is the case for Flux-PIHM (except for direct runoff). This is clearly difficult to represent with lumped parameters, which can help explain the subdued variation in the modeled versus measured NO_3^--N concentration in the stream (Fig. 6).

The quality of Cycles-L predictions depends on both model structure and input data quality. To represent, for example, large N discharge events, accurate input of the amount, timing, and composition of the N amendments is critical. However, the composition of animal manure is highly variable (Griffin et al., 2005), so that there is an inherent variance in the addition of N and other nutrients to fields or watersheds via manure. In this study, manure N input represented 42% of the N input in the 1x N scenario (Table 2), and was on average twice as large as the NO_3^--N watershed discharge. In addition, for the simulations presented here, the prescribed management practices have the same planting dates, tillage dates and practices, and fertilization dates and rates every year, which are approximately correct on average but likely incorrect in any given year of the 16-year simulation period. Therefore using the surveyed management data introduces uncertainty that would reflect in deviations of stream flow and especially NO_3^--N concentration (Fig. 6) independently of the model algorithms. The underestimation of NO_3^--N discharge when using survey data to represent fertilizer inputs (1x) and the improvement through the modeled 1.25x and 1.5x scenarios suggest that N inputs through fertilizer could have been underestimated on average by 30%. Indeed, a mismatch between field survey data on N (and phosphorus) input and that needed to match crop yield and other variables has been reported before (USDA-NRCS, 2012, page 30).

Cycles-L couples a hydrologic model (PIHM), land surface model (Noah LSM), and agroecosystem model (Cycles) together. The interactions among these components are complex and the number of parameters involved is large even when using a conservative approach for model development. Parameter sensitivity in Flux-PIHM has been examined in previous studies (Shi et al., 2014; Xiao et al., 2019), which revealed complex interactions among model parameters and between land surface-subsurface processes that are inherited in Cycles-L. Sensitivity analysis of Cycles-L can help identify critical model parameterization and reveal any potential dependence of model results on grid resolution.

Operationally, it is simple to set up and run 1-D models like a stand alone Cycles 1-D with standardized inputs. Once the soil profile and weather forcing are formatted to conform to requirements, there is no impediment to run the model. Setting up and running 3-D models is less straightforward. While the generation of input files, grid and stream network has been automated in the past for CONUS to provide users a starting point at the HUC12 level (Leonard & Duffy, 2014), automation does not warrant that the setup provides a stable frame to represent hydrology. Often, the grid and stream network setup needs to be streamlined to secure convergence of fluxes and state variables or to avoid resorting to small time steps that slow down execution. However, once a set up is ready, it can be stored, shared, and re-used efficiently, and support running new scenarios or applications that need to combine measurements and modeling (e.g., Drake et al., 2018) with agility.

6 Conclusions

Cycles-L is among the first next generation physically-based spatially-distributed agroecosystem models that can represent landscape processes. The coupling of biogeochemical and hydrologic processes at the catchment scale places this model between 1-D models that simplify terrain and other attributes, and global models that connect atmospheric volumes in 3-D but are underlined by simplified land models. Cycles-L occupies therefore a unique operational space relevant to simulate interventions in the landscape.

In the test case presented here for Central Pennsylvania, Cycles-L simulated well hydrology, grain crops yield, and N exports in the stream, despite some uncertainty in the quality of the input data. Cycles-L retains, therefore, the strengths of Flux-PIHM (Shi et al., 2013) and the 1-D Cycles model (Kemanian et al., 2022). Compared to the uncoupled Flux-PIHM (water discharge) and Cycles (crop yield) models, the predictions of Cycles-L are as good if not improved. The model skill at predicting the impact of topography, soil heterogeneity, and crop management on N fluxes temporally and spatially can expand the domain of *in silico* agroecosystem analysis to landscape levels.

Further progress will depend on continuously balancing the complexity of the model algorithms with concomitant improvements in input quality, to take advantage of increasing computing capacity and to represent landscapes with increasing fidelity. We envision that tools like Cycles-L will become a critical component of the analytical toolkit of both academic and non-academic communities.

Acknowledgments

Funding for this research provided by DoE BETO grant DE-EE0007088/0000, EPA Grant RD835568, NSF-CNHS grant ICER-1517823, and USDA-NIFA Award 2012-68005-19703 and 2020-68012-31824, and the College of Agricultural Sciences at Penn State via USA Hatch Appropriations under Project PEN04571 and Accession 1003346. The NLDAS-2 data used in this study were acquired as part of the mission of NASA's Earth Science Division and archived and distributed by the Goddard Earth Sciences (GES) Data and Information Services Center (DISC).

References

Arnold, J. G., Srinivasan, R., Muttiah, R. S., & Williams, J. R. (1998). Large area hydrologic modeling and assessment. Part I: Model development. *JAWRA Journal of the American Water Resources Association*, *34*(1), 73–89. doi: 10.1111/j.1752-1688.1998.tb05961.x

Ator, S. W., & Garcia, A. M. (2016). Application of SPARROW Modeling to understanding contaminant fate and transport from uplands to streams. *Journal of the American Water Resources Association (JAWRA)*, *52*(3), 685–704. doi: 10.1111/1752-1688.12419

Baker, J. M., Ochsner, T. E., Venterea, R. T., & Griffis, T. J. (2007). Tillage and soil carbon sequestration—What do we really know? *Agriculture, Ecosystems & Environment*, *118*(1), 1–5. doi: 10.1016/j.agee.2006.05.014

Bao, C., Li, L., Shi, Y., & Duffy, C. (2017). Understanding watershed hydrogeochemistry: 1. Development of RT-Flux-PIHM. *Water Resources Research*, *53*(3), 2328–2345. doi: 10.1002/2016WR018934

Basso, B., Bertocco, M., Sartori, L., & Martin, E. C. (2007). Analyzing the effects of climate variability on spatial pattern of yield in a maize–wheat–soybean rotation. *European Journal of Agronomy*, *26*(2), 82–91. doi: 10.1016/j.eja.2006.08.008

Batchelor, W. D., Basso, B., & Paz, J. O. (2002). Examples of strategies to analyze spatial and temporal yield variability using crop models. *European Journal of Agronomy*, *18*(1), 141–158. doi: 10.1016/S1161-0301(02)00101-6

Beaujouan, V., Durand, P., & Ruiz, L. (2001). Modelling the effect of the spatial distribution of agricultural practices on nitrogen fluxes in rural catchments. *Ecological Modelling*, *137*(1), 93–105. doi: 10.1016/S0304-3800(00)00435-X

Bhatt, G., Kumar, M., & Duffy, C. J. (2014). A tightly coupled GIS and distributed hydrologic modeling framework. *Environmental Modelling & Software*, *62*, 70–84. doi: 10.1016/j.envsoft.2014.08.003

Bonilla, C. A., Norman, J. M., & Molling, C. C. (2007). Water erosion estimation in topographically complex landscapes: Model description and first verifications. *Soil Science Society of America Journal*, *71*(5), 1524–1537. doi: 10.2136/sssaj2006.0302

Bonilla, C. A., Norman, J. M., Molling, C. C., Karthikeyan, K. G., & Miller, P. S. (2008). Testing a grid-based soil erosion model across topographically complex landscapes. *Soil Science Society of America Journal*, *72*(6), 1745–1755. doi: 10.2136/sssaj2007.0310

Booker, J. D., Lascano, R. J., Evett, S. R., & Zartman, R. E. (2014). Evaluation of a landscape-scale approach to cotton modeling. *Agronomy Journal*, *106*(6), 2263–2279. doi: 10.2134/agronj14.0202

Booker, J. D., Lascano, R. J., Molling, C. C., Zartman, R. E., & Acosta-Martínez, V. (2015). Temporal and spatial simulation of production-scale irrigated cotton systems. *Precision Agriculture*, *16*(6), 630–653. doi: 10.1007/s11119-015-9397-6

Boote, K. J., Jones, J. W., Hoogenboom, G., & White, J. W. (2010). The role of crop systems simulation in agriculture and environment. *International Journal of Agricultural and Environmental Information Systems (IJAEIS)*, *1*(1), 41–54. doi: 10.4018/jaeis.2010101303

Bryant, R. B., Veith, T. L., Feyereisen, G. W., Buda, A. R., Church, C. D., Folmar, G. J., … Kleinman, P. J. A. (2011). U.S. Department of Agriculture Agricultural Research Service Mahantango Creek Watershed, Pennsylvania, United States: Physiography and history. *Water Resources Research*, *47*, W08701. doi: 10.1029/2010WR010056

Buda, A. R., Feyereisen, G. W., Veith, T. L., Folmar, G. J., Bryant, R. B., Church, C. D., … Kleinman, P. J. A. (2011). U.S. Department of Agriculture Agricultural Research Service Mahantango Creek Watershed, Pennsylvania, United

States: Long-term stream discharge database. *Water Resources Research*, *47*(8). doi: 10.1029/2010WR010059

Campbell, G. S. (1985). *Soil physics with BASIC: transport models for soil-plant systems*. Amsterdam: Elsevier.

Castaño-Sánchez, J. P., Rotz, C. A., Karsten, H. D., & Kemanian, A. R. (2020). Elevated atmospheric carbon dioxide effects on maize and alfalfa in the Northeast US: A comparison of model predictions and observed data. *Agricultural and Forest Meteorology*, *291*, 108093. doi: 10.1016/j.agrformet.2020.108093

Chen, E., & Mackay, D. (2004). Effects of distribution-based parameter aggregation on a spatially distributed agricultural nonpoint source pollution model. *Journal of Hydrology*, *295*(1), 211–224. doi: 10.1016/j.jhydrol.2004.03.029

Chen, F., & Dudhia, J. (2001). Coupling an advanced land surface–hydrology model with the Penn State–NCAR MM5 modeling system. Part I: Model implementation and sensitivity. *Monthly Weather Review*, *129*(4), 569–585. doi: 10.1175/1520-0493(2001)129⟨0569:CAALSH⟩2.0.CO;2

Church, C. D., Veith, T. L., Folmar, G. J., Buda, A. R., Feyereisen, G. W., Bryant, R. B., ... Kleinman, P. J. A. (2011). U.S. Department of Agriculture Agricultural Research Service Mahantango Creek Watershed, Pennsylvania, United States: Long-term water quality database. *Water Resources Research*, *47*(8), W08704. doi: 10.1029/2010WR010060

Collins, E. L., Sanchez, G. M., Terando, A., Stillwell, C. C., Mitasova, H., Sebastian, A., & Meentemeyer, R. K. (2022). Predicting flood damage probability across the conterminous United States. *Environmental Research Letters*, *17*(3), 034006. doi: 10.1088/1748-9326/ac4f0f

Confalonieri, R., Orlando, F., Paleari, L., Stella, T., Gilardelli, C., Movedi, E., ... Acutis, M. (2016). Uncertainty in crop model predictions: What is the role of users? *Environmental Modelling & Software*, *81*, 165–173. doi: 10.1016/j.envsoft.2016.04.009

Cowan, I. R. (1978). Stomatal behaviour and environment. In R. D. Preston & H. W. Woolhouse (Eds.), (Vol. 4, pp. 117–228). Academic Press. doi: 10.1016/S0065-2296(08)60370-5

Cowan, I. R. (1982). Regulation of water use in relation to carbon gain in higher plants. In O. L. Lange, P. S. Nobel, C. B. Osmond, & H. Ziegler (Eds.), *Physiological plant ecology ii: Water relations and carbon assimilation* (pp. 589–613). Berlin, Heidelberg: Springer Berlin Heidelberg. doi: 10.1007/978-3-642-68150-9_18

Crow, W. T., Milak, S., Moghaddam, M., Tabatabaeenejad, A., Member, S., Jaruwatanadilok, S., ... Cuenca, R. H. (2018). Spatial and Temporal Variability of Root-Zone Soil Moisture Acquired From Hydrologic Modeling and AirMOSS P -Band Radar. *IEEE Journal of Selected Topics in Applied Earth Observations and Remote Sensing*, *PP*(12), 1–13. doi: 10.1109/JSTARS.2018.2865251

De Schepper, G., Therrien, R., Refsgaard, J. C., & Hansen, A. L. (2015). Simulating coupled surface and subsurface water flow in a tile-drained agricultural catchment. *Journal of Hydrology*, *521*, 374–388. doi: 10.1016/j.jhydrol.2014.12.035

de Saint-Venant, B. (1871). Theory of unsteady water flow with application to floods and to propagation of tides in river channels. *Proceedings of French Academy of Science*, *73*, 148–154.

Drake, C. W., Jones, C. S., Schilling, K. E., Amado, A. A., & Weber, L. J. (2018). Estimating nitrate-nitrogen retention in a large constructed wetland using high-frequency, continuous monitoring and hydrologic modeling. *Ecological Engineering*, *117*, 69–83. doi: 10.1016/j.ecoleng.2018.03.014

Ek, M. B., Mitchell, K. E., Lin, Y., Rogers, E., Grunmann, P., Koren, V., ... Tarpley, J. D. (2003). Implementation of Noah land surface model advances in the National Centers for Environmental Prediction operational mesoscale Eta model. *Journal of Geophysical Research*, *108*(D22), 8851. doi: 10.1029/2002JD003296

Foley, J. A., Prentice, I. C., Ramankutty, N., Levis, S., Pollard, D., Sitch, S., & Haxeltine, A. (1996). An integrated biosphere model of land surface processes, terrestrial carbon balance, and vegetation dynamics. *Global Biogeochemical Cycles*, *10*(4), 603–628. doi: 10.1029/96GB02692

Francesconi, W., Smith, D. R., Heathman, G. C., Wang, X., & Williams, C. O. (2014). Monitoring and APEX Modeling of no-till and reduced-till in tile-drained agricultural landscapes for water quality. *Transactions of the American Society of Agricultural and Biological Engineers*, *57*(3), 777–789. doi: 10.13031/trans.57.10332

Frank, S., Fürst, C., Koschke, L., & Makeschin, F. (2012). A contribution towards a transfer of the ecosystem service concept to landscape planning using landscape metrics. *Ecological Indicators*, *21*, 30–38. doi: 10.1016/j.ecolind.2011.04.027

Gassman, P. W., Williams, J. R., Wang, X., Saleh, A., Osei, E., Hauck, L. M., … Flowers, D. J. (2010). The Agricultural Policy/Environmental eXtender (APEX) Model: An emerging tool for landscape and watershed environmental analyses. *Transactions of the American Society of Agricultural and Biological Engineers*, *53*(3), 711–740. doi: 10.13031/2013.30078

Gil, Y., Garijo, D., Khider, D., Knoblock, C. A., Ratnakar, V., Osorio, M., … Shu, L. (2021). Artificial intelligence for modeling complex systems: Taming the complexity of expert models to improve decision making. *ACM Trans. Interact. Intell. Syst.*, *11*(2). doi: 10.1145/3453172

Griffin, T. S., He, Z., & Honeycutt, C. W. (2005). Manure composition affects net transformation of nitrogen from dairy manures. *Plant and Soil*, *273*(1), 29–38. doi: 10.1007/s11104-004-6473-5

Groffman, P. M., Butterbach-Bahl, K., Fulweiler, R. W., Gold, A. J., Morse, J. L., Stander, E. K., … Vidon, P. (2009). Challenges to incorporating spatially and temporally explicit phenomena (hotspots and hot moments) in denitrification models. *Biogeochemistry*, *93*(1), 49–77. doi: 10.1007/s10533-008-9277-5

Hill, A. R., Devito, K. J., & Vidon, P. G. (2014). Long-term nitrate removal in a stream riparian zone. *Biogeochemistry*, *121*(2), 425–439. doi: 10.1007/s10533-014-0010-2

Hindmarsh, A. C., Brown, P. N., Grant, K. E., Lee, S. L., Serban, R., Shumaker, D. E., & Woodward, C. S. (2005). SUNDIALS: Suite of nonlinear and differential/algebraic equation solvers. *ACM Transactions on Mathematical Software*, *31*(3), 363—-396.

Hirt, C. C., Veith, T. L., Collick, A. S., Yetter, S. E., & Brooks, R. P. (2020). Headwater stream condition and nutrient runoff: Relating SWAT to empirical ecological measures in an agricultural watershed in Pennsylvania. *Journal of Environmental Quality*, *49*(3), 557–568. doi: 10.1002/jeq2.20032

Hladik, M. L., & Kolpin, D. W. (2015). First national-scale reconnaissance of neonicotinoid insecticides in streams across the USA. *Environmental Chemistry*, *13*(1), 12–20. doi: 10.1071/EN15061

Jacob, D., Petersen, J., Eggert, B., Alias, A., Christensen, O. B., Bouwer, L. M., … Yiou, P. (2014). EURO-CORDEX: New high-resolution climate change projections for European impact research. *Regional Environmental Change*, *14*(2), 563–578. doi: 10.1007/s10113-013-0499-2

Jepsen, S. M., Harmon, T. C., & Shi, Y. (2016). Watershed model calibration to the base flow recession curve with and without evapotranspiration effects. *Water Resources Research*, *52*(4), 2919–2933. doi: 10.1002/2015WR017827

Katul, G., Manzoni, S., Palmroth, S., & Oren, R. (2009). A stomatal optimization theory to describe the effects of atmospheric CO_2 on leaf photosynthesis and transpiration. *Annals of Botany*, *105*(3), 431–442. doi: 10.1093/aob/mcp292

Kemanian, A. R., Duckworth, P., & Williams, J. R. (2009). A spatially distributed modeling approach for precision conservation and agroecosystem design. *Proc. 2nd Biennial Int. Symp. Farming Systems Design*, 153–154.

Kemanian, A. R., Shi, Y., White, C. M., Montes, F., Stöckle, C. O., Huggins, D. R., ... Rozum, R. K. N. (2022). The cycles agroecosystem model: Fundamentals, testing, and applications. *Agricultural and Forest Meteorology*, *Under review*.

Kemanian, A. R., & Stöckle, C. O. (2010). C-Farm: A simple model to evaluate the carbon balance of soil profiles. *European Journal of Agronomy*, *32*(1), 22–29. doi: 10.1016/j.eja.2009.08.003

Kirchner, J. W. (2006). Getting the right answers for the right reasons: Linking measurements, analyses, and models to advance the science of hydrology. *Water Resources Research*, *42*(3), W03S04. doi: 10.1029/2005WR004362

Koch, J., Cornelissen, T., Fang, Z., Bogena, H., Diekkrüger, B., Kollet, S., & Stisen, S. (2016). Inter-comparison of three distributed hydrological models with respect to seasonal variability of soil moisture patterns at a small forested catchment. *Journal of Hydrology*, *533*, 234–249. doi: 10.1016/j.jhydrol.2015.12.002

Kucharik, C. J., Foley, J. A., Delire, C., Fisher, V. A., Coe, M. T., Lenters, J. D., ... Gower, S. T. (2000). Testing the performance of a dynamic global ecosystem model: Water balance, carbon balance, and vegetation structure. *Global Biogeochemical Cycles*, *14*(3), 795–825. doi: 10.1029/1999GB001138

Kumar, M., Bhatt, G., & Duffy, C. J. (2010). An object-oriented shared data model for GIS and distributed hydrologic models. *International Journal of Geographical Information Science*, *24*(7), 1061–1079. doi: 10.1080/13658810903289460

Leonard, L., & Duffy, C. J. (2014). Automating data-model workflows at a level 12 HUC scale: Watershed modeling in a distributed computing environment. *Environmental Modelling & Software*, *61*, 174–190. doi: 10.1016/j.envsoft.2014.07.015

Lu, H., Bryant, R. B., Buda, A. R., Collick, A. S., Folmar, G. J., & Kleinman, P. J. A. (2015). Long-term trends in climate and hydrology in an agricultural, headwater watershed of central Pennsylvania, USA. *Journal of Hydrology: Regional Studies*, *4*, 713–731. doi: 10.1016/j.ejrh.2015.10.004

McConnell, C. A., Kaye, J. P., & Kemanian, A. R. (2020). Reviews and syntheses: Ironing out wrinkles in the soil phosphorus cycling paradigm. *Biogeosciences*, *17*(21), 5309–5333. doi: 10.5194/bg-17-5309-2020

McLellan, E. L., Cassman, K. G., Eagle, A. J., Woodbury, P. B., Sela, S., Tonitto, C., ... van Es, H. M. (2018). The Nitrogen balancing act: Tracking the environmental performance of food production. *BioScience*, *68*(3), 194–203. doi: 10.1093/biosci/bix164

Molling, C. C., Strikwerda, J. C., Norman, J. M., Rodgers, C. A., Wayne, R., Morgan, C. L., ... Mecikalski, J. R. (2005). Distributed runoff formulation designed for a precision agricultural landscape modeling system. *Journal of the American Water Resources Association*, *41*(6), 1289–1313. doi: 10.1111/j.1752-1688.2005.tb03801.x

Pabich, W. J., Valiela, I., & Hemond, H. F. (2001). Relationship between DOC concentration and vadose zone thickness and depth below water table in groundwater of Cape Cod, U.S.A. *Biogeochemistry*, *55*(3), 247–268. doi: 10.1023/A:1011842918260

PASDA. (2022). *Pennsylvania Spatial Data Access.* Retrieved 2022-04-25, from `https://www.pasda.psu.edu/`

Pineux, N., Lisein, J., Swerts, G., Bielders, C. L., Lejeune, P., Colinet, G., & Degré, A. (2017). Can DEM time series produced by UAV be used to quantify diffuse erosion in an agricultural watershed? *Geomorphology*, *280*, 122–136. doi: 10.1016/j.geomorph.2016.12.003

Pionke, H. B., Gburek, W. J., & Sharpley, A. N. (2000). Critical source area controls on water quality in an agricultural watershed located in the Chesapeake

Basin. *Ecological Engineering*, *14*(4), 325–335. doi: https://doi.org/10.1016/S0925-8574(99)00059-2

Pravia, M. V., Kemanian, A. R., Terra, J. A., Shi, Y., Macedo, I., & Goslee, S. (2019). Soil carbon saturation, productivity, and carbon and nitrogen cycling in crop-pasture rotations. *Agricultural Systems*, *171*(December 2017), 13–22. doi: 10.1016/j.agsy.2018.11.001

Qu, Y., & Duffy, C. J. (2007). A semidiscrete finite volume formulation for multiprocess watershed simulation. *Water Resources Research*, *43*(8), W08419. doi: 10.1029/2006WR005752

Redder, B. W., Kennedy, C. D., Buda, A. R., Folmar, G., & Boyer, E. W. (2021). Groundwater contributions of flow and nitrogen in a headwater agricultural watershed. *Hydrological Processes*, *35*(5), e14179. doi: 10.1002/hyp.14179

Rodell, M., Houser, P. R., Jambor, U., Gottschalck, J., Mitchell, K., Meng, C.-J., ... Others (2004). The global land data assimilation system. *Bulletin of the American Meteorological Society*, *85*(3), 381–394. doi: 10.1175/BAMS-85-3-381

Saarikko, R. A. (2000). Applying a site based crop model to estimate regional yields under current and changed climates. *Ecological Modelling*, *131*(2), 191–206. doi: 10.1016/S0304-3800(00)00257-X

Saha, D., Kaye, J. P., Bhowmik, A., Bruns, M. A., Wallace, J. M., & Kemanian, A. R. (2021). Organic fertility inputs synergistically increase denitrification-derived nitrous oxide emissions in agroecosystems. *Ecological Applications*, *31*(7), e02403. doi: 10.1002/eap.2403

Saha, D., Rau, B. M., Kaye, J. P., Montes, F., Adler, P. R., & Kemanian, A. R. (2017). Landscape control of nitrous oxide emissions during the transition from conservation reserve program to perennial grasses for bioenergy. *GCB Bioenergy*, *9*(4), 783–795. doi: 10.1111/gcbb.12395

Shi, Y., Baldwin, D. C., Davis, K. J., Yu, X., Duffy, C. J., & Lin, H. (2015). Simulating high-resolution soil moisture patterns in the Shale Hills watershed using a land surface hydrologic model. *Hydrological Processes*, *29*(21), 4624–4637. doi: 10.1002/hyp.10593

Shi, Y., Davis, K. J., Duffy, C. J., & Yu, X. (2013). Development of a Coupled Land Surface Hydrologic Model and Evaluation at a Critical Zone Observatory. *Journal of Hydrometeorology*, *14*(5), 1401–1420. doi: 10.1175/JHM-D-12-0145.1

Shi, Y., Davis, K. J., Zhang, F., & Duffy, C. J. (2014). Evaluation of the Parameter Sensitivities of a Coupled Land Surface Hydrologic Model at a Critical Zone Observatory. *Journal of Hydrometeorology*, *15*(1), 279–299. doi: 10.1175/JHM-D-12-0177.1

Shi, Y., Eissenstat, D. M., He, Y., & Davis, K. J. (2018). Using a spatially-distributed hydrologic biogeochemistry model with a nitrogen transport module to study the spatial variation of carbon processes in a Critical Zone Observatory. *Ecological Modelling*, *380*, 8–21. doi: 10.1016/j.ecolmodel.2018.04.007

Stafford, J. V. (2000). Implementing precision agriculture in the 21st century. *Journal of Agricultural and Engineering Research*, *76*(3), 267–275. doi: 10.1006/jaer.2000.0577

Stöckle, C. O., & Kemanian, A. R. (2020). Can crop models identify critical gaps in genetics, environment, and management interactions? *Frontiers in Plant Science*, *11*, 737. doi: 10.3389/fpls.2020.00737

Stöckle, C. O., Kemanian, A. R., Nelson, R. L., Adam, J. C., Sommer, R., & Carlson, B. (2014). CropSyst model evolution: From field to regional to global scales and from research to decision support systems. *Environmental Modelling & Software*, *62*, 361–369. doi: 10.1016/j.envsoft.2014.09.006

Tague, C. L., & Band, L. E. (2004). RHESSys: Regional Hydro-Ecologic Simulation System—An object-oriented approach to spatially distributed modeling of carbon, water, and nutrient cycling. *Earth Interactions*, *8*(19), 1–42. doi:

10.1175/1087-3562(2004)8⟨1:RRHSSO⟩2.0.CO;2

Tarboton, D. G. (2015). *TauDEM -Terrain Analysis Using Digital Elevation Models. Version 5.* Retrieved 2022-04-25, from https://hydrology.usu.edu/taudem/taudem5/index.html

Tarboton, D. G., Bras, R. L., & Rodriguez-Iturbe, I. (1991). On the extraction of channel networks from digital elevation data. *Hydrological Processes*, *5*(1), 81–100. doi: 10.1002/hyp.3360050107

Tarboton, D. G., Schreuders, K. A. T., Watson, D. W., & Baker, M. E. (2009). Generalized terrain-based flow analysis of digital elevation models. In *Proceedings of the 18th world imacs congress and modsim09 international congress on modelling and simulation, cairns, australia* (Vol. 20002006, pp. 2377–2383). Cairns, Australia.

Tenreiro, T. R., García-Vila, M., Gómez, J. A., Jimenez-Berni, J. A., & Fereres, E. (2020). Water modelling approaches and opportunities to simulate spatial water variations at crop field level. *Agricultural Water Management*, *240*, 106254. doi: 10.1016/j.agwat.2020.106254

USDA-NRCS. (2012). *Assessment of the effects of conservation practices on cultivated cropland in the Upper Mississippi River Basin (Revised CEAP Report 2012)* (Tech. Rep.).

Van Liew, M. W., Wortmann, C. S., Moriasi, D. N., King, K. W., Flanagan, D. C., Veith, T. L., … Tomer, M. D. (2017). Evaluating the APEX model for simulating streamflow and water quality on ten Aaricultural watersheds in the U.S. *Transactions of the American Society of Agricultural and Biological Engineers*, *60*(1), 123–146. doi: 10.13031/trans.11903

Veith, T. L., Richards, J. E., Goslee, S. C., Collick, A. S., Bryant, R. B., Miller, D. A., … Kleinman, P. J. (2015). Navigating spatial and temporal complexity in developing a long-term land use database for an agricultural watershed. *Journal of Soil and Water Conservation*, *70*(5), 288–296. doi: 10.2489/jswc.70.5.288

Wallace, C. D., Sawyer, A. H., Soltanian, M. R., & Barnes, R. T. (2020). Nitrate removal within heterogeneous riparian aquifers under tidal influence. *Geophysical Research Letters*, *47*(10), e2019GL085699. doi: 10.1029/2019GL085699

Wang, C., Hou, J., Miller, D., Brown, I., & Jiang, Y. (2019). Flood risk management in sponge cities: The role of integrated simulation and 3D visualization. *International Journal of Disaster Risk Reduction*, *39*, 101139. doi: 10.1016/j.ijdrr.2019.101139

Wang, X., Kemanian, A. R., & Williams, J. R. (2011). Special features of the EPIC and APEX modeling package and procedures for parameterization, calibration, validation, and applications. In L. R. Ahuja & L. Ma (Eds.), *Methods of introducing system models into agricultural research* (pp. 177–208). John Wiley & Sons, Ltd. doi: 10.2134/advagricsystmodel2.c6

Ward, N. K., Maureira, F., Stöckle, C. O., Brooks, E. S., Painter, K. M., Yourek, M. A., & Gasch, C. K. (2018). Simulating field-scale variability and precision management with a 3D hydrologic cropping systems model. *Precision Agriculture*, *19*(2), 293–313. doi: 10.1007/s11119-017-9517-6

Wigmosta, M. S., & Lettenmaier, D. P. (1999). A comparison of simplified methods for routing topographically driven subsurface flow. *Water Resources Research*, *35*(1), 255–264. doi: 10.1029/1998WR900017

Williams, J. R. (1990). The Erosion-Productivity Impact Calculator (EPIC) model: A case history. *Philosophical Transactions of the Royal Society of London. Series B: Biological Sciences*, *329*(1255), 421–428. doi: 10.1098/rstb.1990.0184

Williams, M. R., Buda, A. R., Elliott, H. A., Singha, K., & Hamlett, J. (2015). Influence of riparian seepage zones on nitrate variability in two agricultural headwater streams. *Journal of the American Water Resources Association (JAWRA)*, *51*(4), 883–897. doi: 10.1111/1752-1688.12335

Woodbury, P. B., Kemanian, A. R., Jacobson, M., & Langholtz, M. (2018). Improving water quality in the Chesapeake Bay using payments for ecosystem services for perennial biomass for bioenergy and biofuel production. *Biomass and Bioenergy*, *114*, 132–142. doi: 10.1016/j.biombioe.2017.01.024

Xia, Y., Mitchell, K., Ek, M., Sheffield, J., Cosgrove, B., Wood, E., … Mocko, D. (2012, feb). Continental-scale water and energy flux analysis and validation for the North American Land Data Assimilation System project phase 2 (NLDAS-2): 1. Intercomparison and application of model products. *Journal of Geophysical Research*, *117*, D03109. doi: 10.1029/2011JD016048

Xiao, D., Shi, Y., Brantley, S. L., Forsythe, B., DiBiase, R., Davis, K., & Li, L. (2019). Streamflow generation from catchments of contrasting lithologies: The role of soil properties, topography, and catchment size. *Water Resources Research*, *55*(11), 9234–9257. doi: 10.1029/2018WR023736

Zhai, Z., Martínez, J. F., Beltran, V., & Martínez, N. L. (2020). Decision support systems for agriculture 4.0: Survey and challenges. *Computers and Electronics in Agriculture*, *170*, 105256. doi: 10.1016/j.compag.2020.105256

Zhang, Y., Li, W., Sun, G., Miao, G., Noormets, A., Emanuel, R., & King, J. S. (2018). Understanding coastal wetland hydrology with a new regional-scale, process-based hydrological model. *Hydrological Processes*, *32*(20), 3158–3173. doi: 10.1002/hyp.13247

Zheng, W., Lamačová, A., Yu, X., Krám, P., Hruška, J., Zahradníček, P., … Farda, A. (2021). Assess hydrological responses to a warming climate at the Lysina Critical Zone Observatory in Central Europe. *Hydrological Processes*, *35*(9), e14281. doi: 10.1002/hyp.14281

Zhi, W., Shi, Y., Wen, H., Saberi, L., Ng, G.-H. C., Sadayappan, K., … Li, L. (2022). BioRT-Flux-PIHM v1.0: A biogeochemical reactive transport model at the watershed scale. *Geoscientific Model Development*, *15*(1), 315–333. doi: 10.5194/gmd-15-315-2022

Figure 1.

Flux-PIHM
Cycles
Precipitation and irrigation
Solar and longwave radiation
Transpiration
Canopy evaporation
Sensible heat flux
Soil evaporation
Snow sublimation
Surface flow
Infiltration
Soil heat flux
Unsaturated zone
Vertical soil water flow
Recharge and capillary rise
Saturated zone
Lateral saturated flow
Channel flow
Daily meteorological condition
Soil temperature
Soil moisture
Snow cover
Vertical soil water flow
Lateral saturated flow
Evapotranspiration
(replaces corresponding
functions in Flux-PIHM)
WATER
S_t, L_i
S_r, L_o, H, λE, G
λE, Q, W_o
PP, I, W_t
ENERGY
CARBON
CO_2, C_h
CO_2, C_r
N_2, NH_3, NH_4, NO_3, N_r
N_2, NH_3, NH_4, NO_3, N_2O, N_h
NITROGEN

Figure 2.

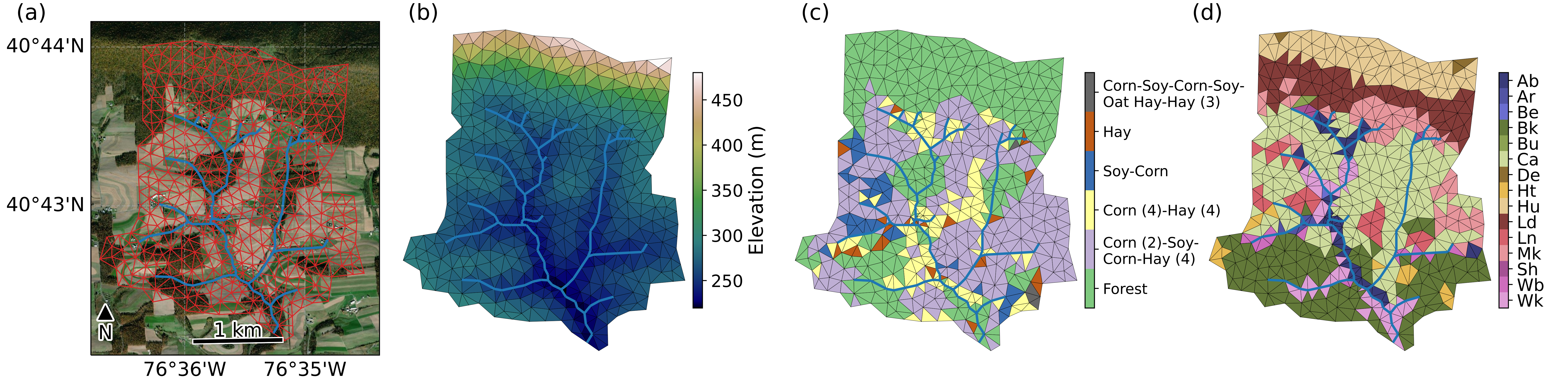

(a)
40°44'N
40°43'N
N
1 km
76°36'W
76°35'W
(b)
Elevation (m)
450
400
350
300
250
(c)
Corn-Soy-Corn-Soy-Oat Hay-Hay (3)
Hay
Soy-Corn
Corn (4)-Hay (4)
Corn (2)-Soy-Corn-Hay (4)
Forest
(d)
Ab
Ar
Be
Bk
Bu
Ca
De
Ht
Hu
Ld
Ln
Mk
Sh
Wb
Wk

Figure 3.

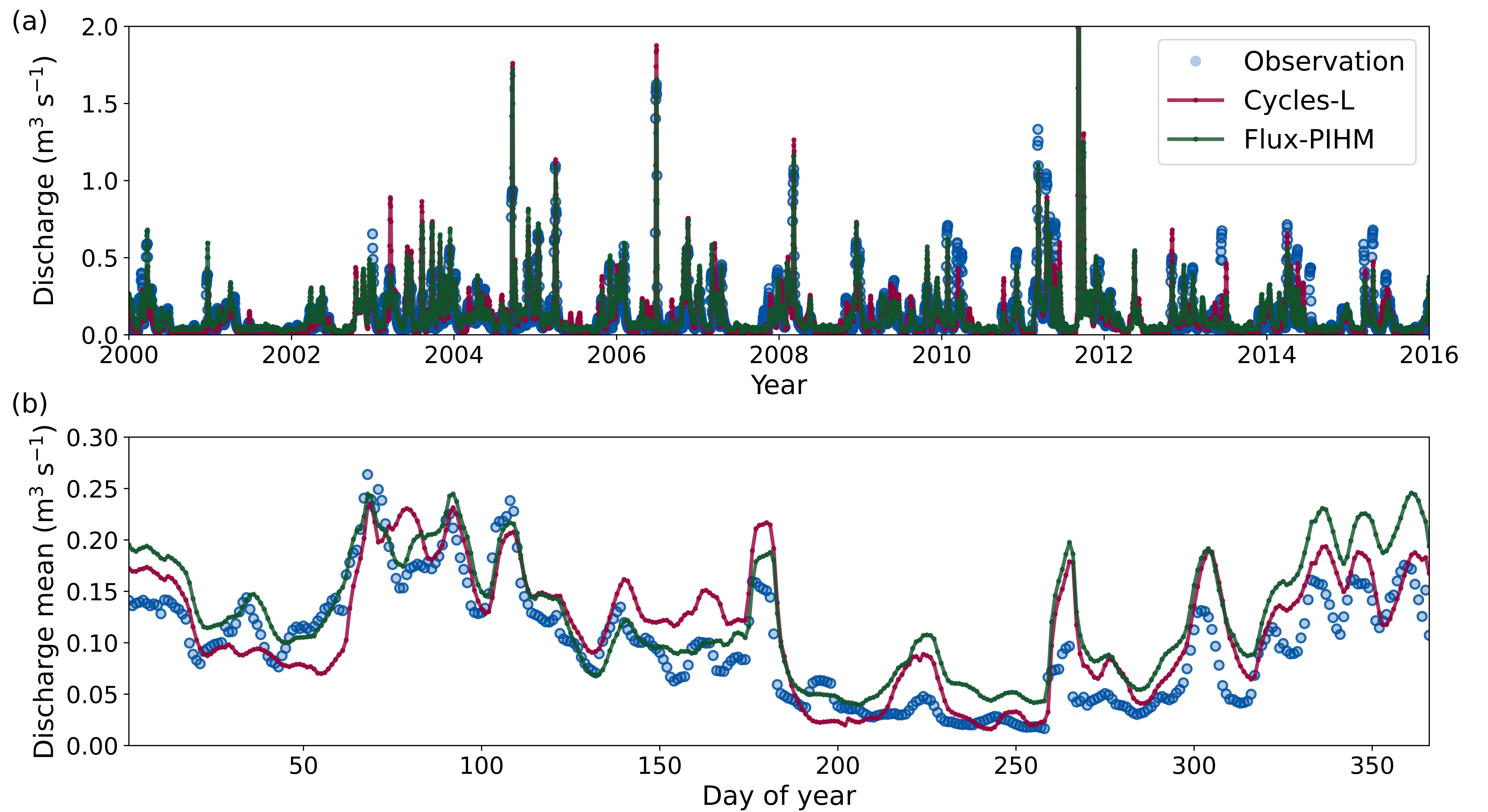

(a)
Discharge (m^3 s^{-1})
0.0
0.5
1.0
1.5
2.0
2000
2002
2004
2006
2008
2010
2012
2014
2016
Year
Observation
Cycles-L
Flux-PIHM
(b)
Discharge mean (m^3 s^{-1})
0.00
0.05
0.10
0.15
0.20
0.25
0.30
50
100
150
200
250
300
350
Day of year

Figure 4.

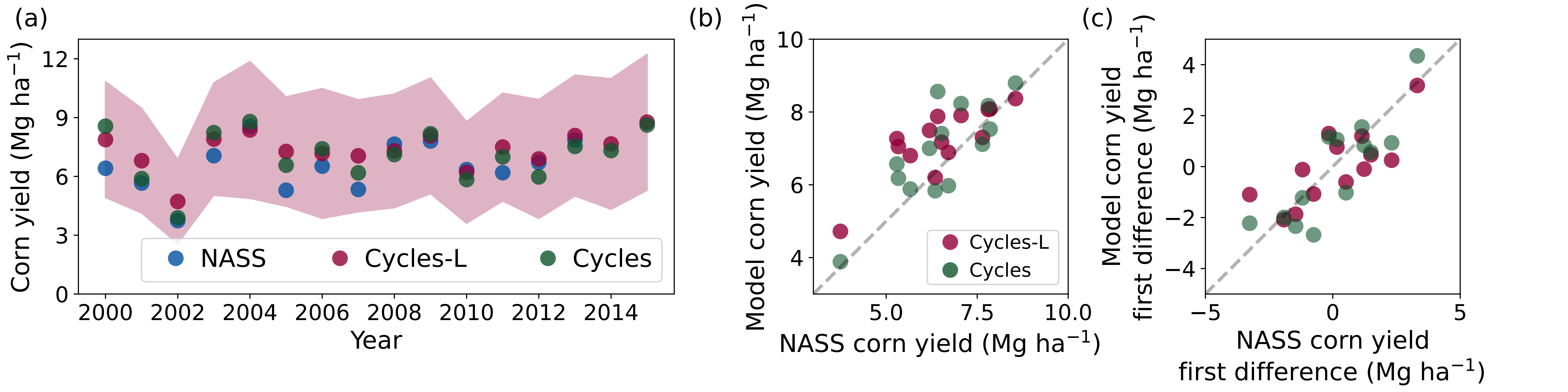

(a)
Corn yield (Mg ha^{-1})
0
3
6
9
12
2000
2002
2004
2006
2008
2010
2012
2014
Year
NASS
Cycles-L
Cycles
(b)
Model corn yield (Mg ha^{-1})
4
6
8
10
5.0
7.5
10.0
NASS corn yield (Mg ha^{-1})
Cycles-L
Cycles
(c)
Model corn yield
first difference (Mg ha^{-1})
−4
−2
0
2
4
−5
0
5
NASS corn yield
first difference (Mg ha^{-1})

Figure 5.

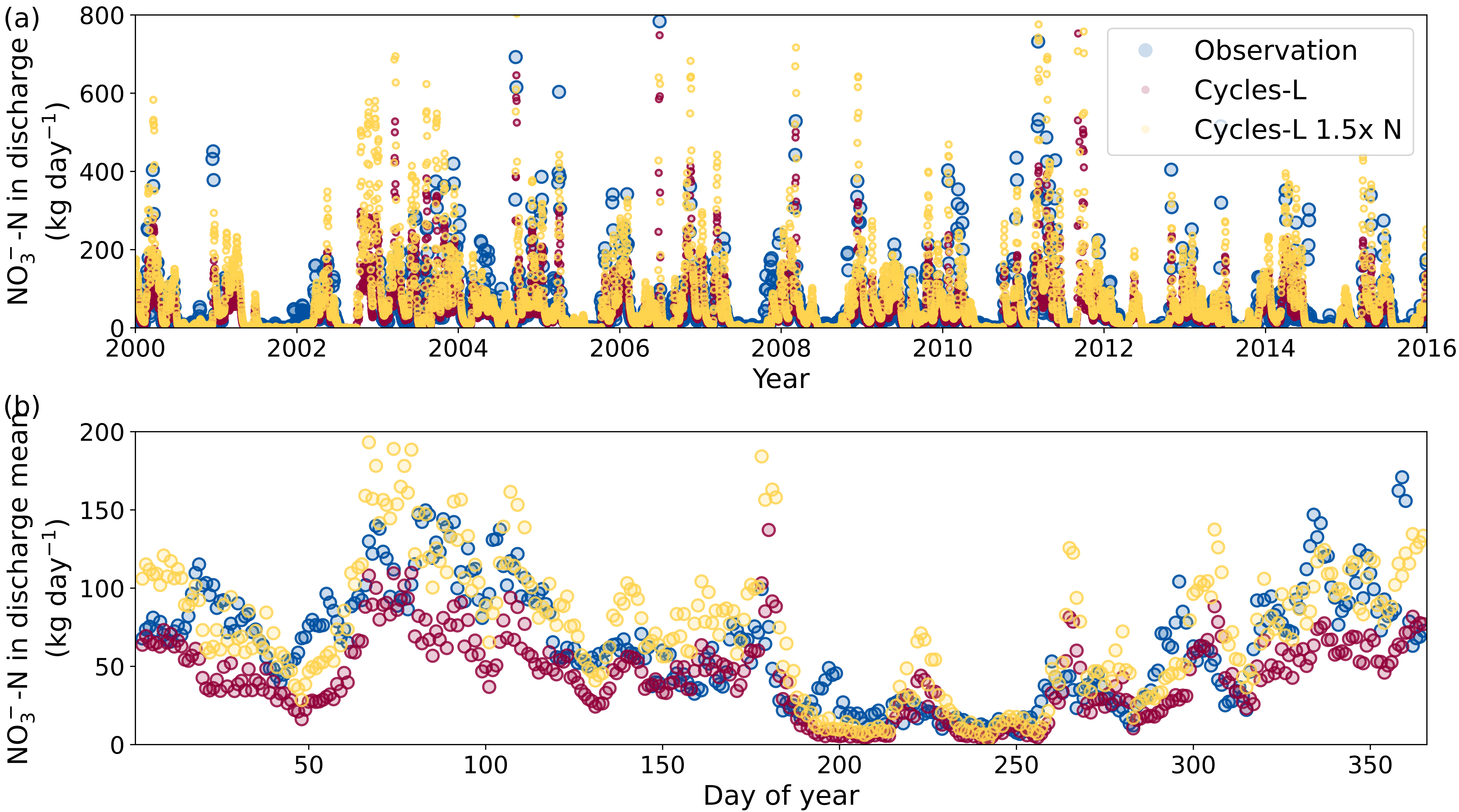

(a)
NO_3^- -N in discharge (kg day^{-1})
Observation
Cycles-L
Cycles-L 1.5x N
Year
(b)
NO_3^- -N in discharge mean (kg day^{-1})
Day of year

Figure 6.

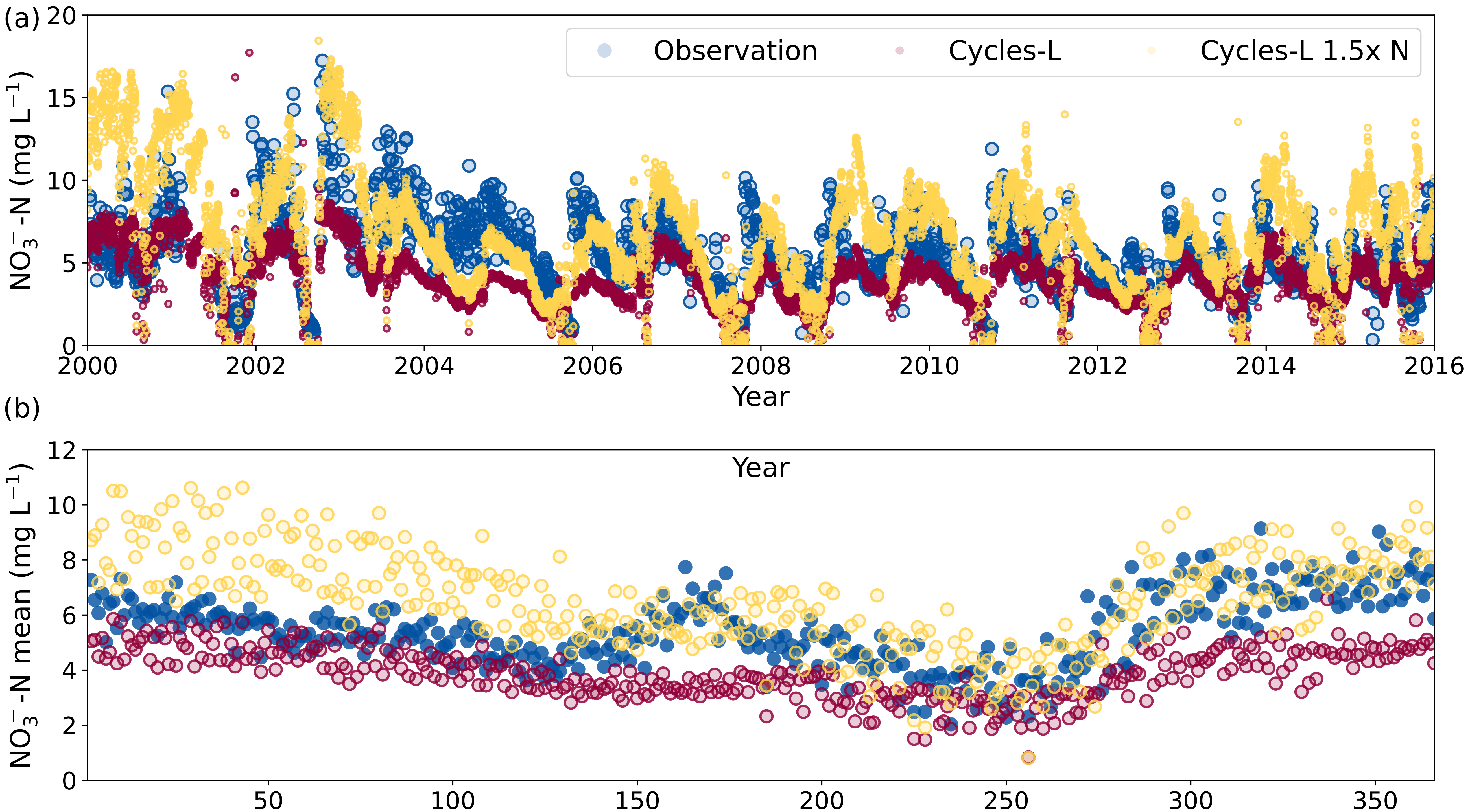

(a)
Observation
Cycles-L
Cycles-L 1.5x N
NO_3^--N (mg L^{-1})
0
5
10
15
20
2000
2002
2004
2006
2008
2010
2012
2014
2016
Year
(b)
Year
NO_3^--N mean (mg L^{-1})
0
2
4
6
8
10
12
50
100
150
200
250
300
350

Figure 7.

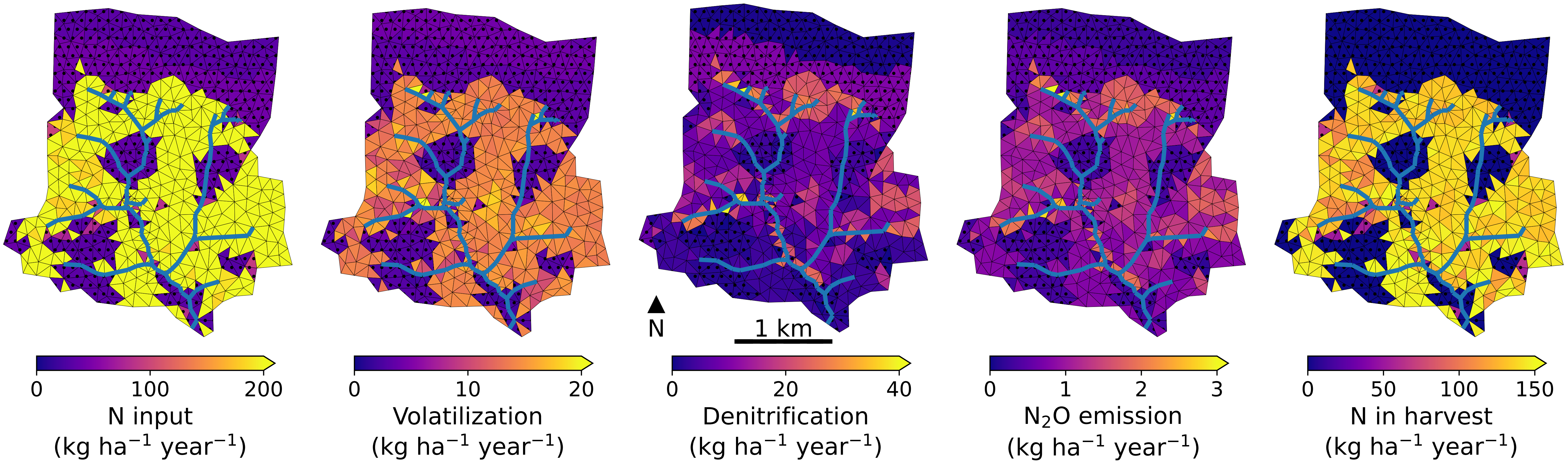
N
1 km
0 100 200
N input
(kg ha^{-1} year^{-1})
0 10 20
Volatilization
(kg ha^{-1} year^{-1})
0 20 40
Denitrification
(kg ha^{-1} year^{-1})
0 1 2 3
N_2O emission
(kg ha^{-1} year^{-1})
0 50 100 150
N in harvest
(kg ha^{-1} year^{-1})

Figure 8.

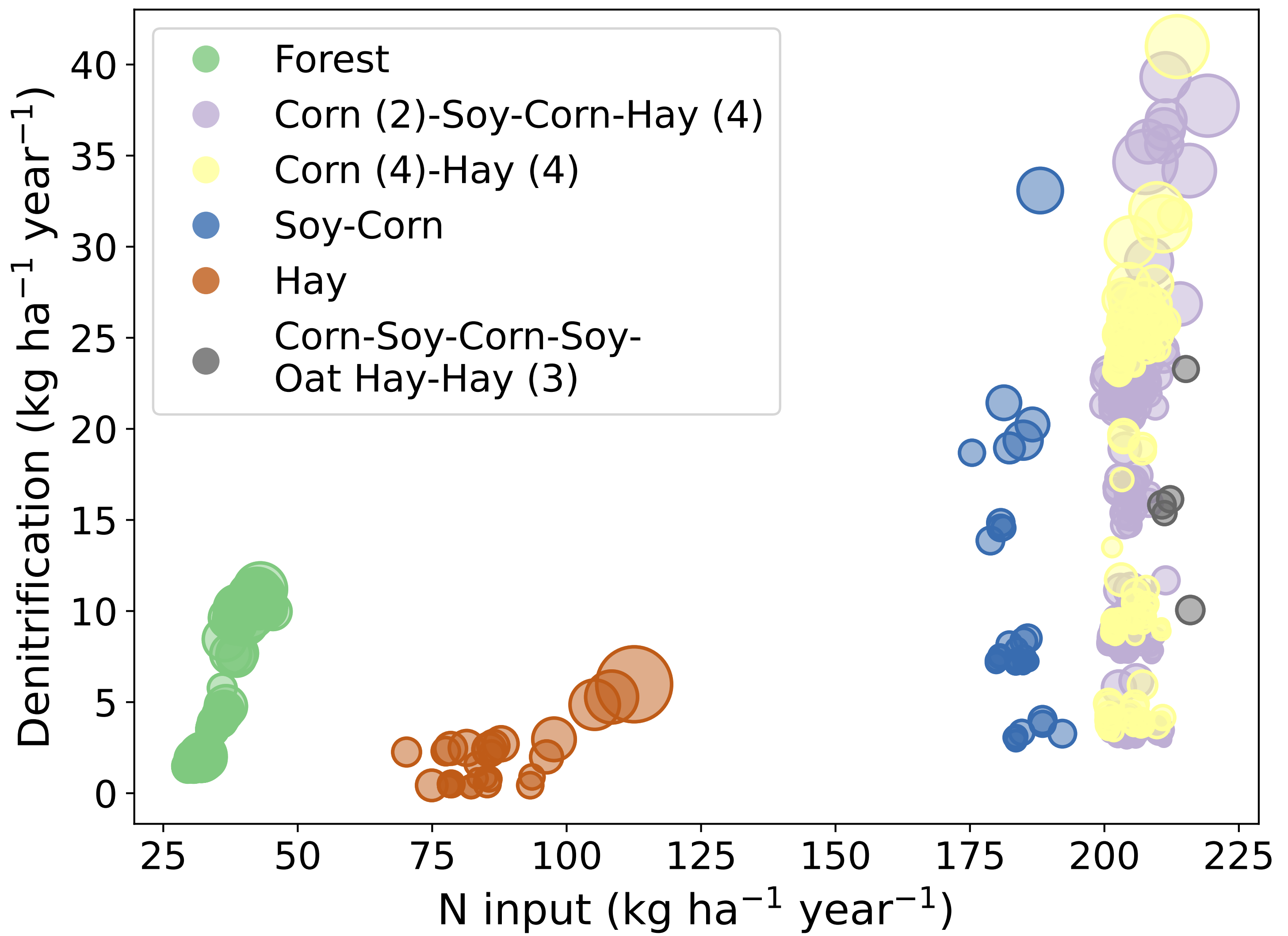
Forest
Corn (2)-Soy-Corn-Hay (4)
Corn (4)-Hay (4)
Soy-Corn
Hay
Corn-Soy-Corn-Soy-Oat Hay-Hay (3)
Denitrification (kg ha^{-1} year^{-1})
N input (kg ha^{-1} year^{-1})
0
5
10
15
20
25
30
35
40
25
50
75
100
125
150
175
200
225